

Ionicity Phase Diagram of Trifluoromethyl-TCNQ (CF_3TCNQ) Charge-Transfer Solids

Gunzi Saito,*[1,2] Hideo Ikegami,[2,†] Yukihiro Yoshida,[1,2] Olga O. Drozdova,[2,††] Kazukuni Nishimura,[2,†††] Sachio Horiuchi,[2,††††] Hideki Yamochi,[3] Akihiro Otsuka,[3] Takaaki Hiramatsu,[3,4] Mitsuhiko Maesato,[2] Takayoshi Nakamura,[5] Tomoyuki Akutagawa,[5,†††††] and Toru Yumoto[5,††††††]

[1]Research Institute, Meijo University, 1-501 Shiogamaguchi, Tempaku-ku, Nagoya 468-8502

[2]Division of Chemistry, Graduate School of Science, Kyoto University, Sakyo-ku, Kyoto 606-8502

[3]Research Center for Low Temperature and Materials Sciences, Kyoto University, Sakyo-ku, Kyoto 606-8501

[4]Institute for Integrated Cell-Material Sciences, Kyoto University, Sakyo-ku, Kyoto 606-8501

[5]Research Institute for Electronic Science and Graduate School of Environmental Earth Science, Hokkaido University, Sapporo 060-0808

Received April 9, 2010; E-mail: gsaito@ccmfs.meijo-u.ac.jp

A series of charge-transfer (CT) solids of trifluoromethyl-7,7,8,8-tetracyanoquinodimethane (CF_3TCNQ) with various electron donor molecules were prepared and their IR and UV–vis–near-IR spectra and electrical conductivity were measured. The information was applied to produce an ionicity phase diagram of CF_3TCNQ CT solids. A boundary for ionicity of CF_3TCNQ was found in combination with donor molecules of dibenzo[*c*,*d*]phenothiazine, diaminodurene, or dibenzotetrathiafulvalene (DBTTF). With stronger donors than DBTTF, the CF_3TCNQ molecules were fully ionized and acted as a counter anion. No conductors with partially charged CF_3TCNQ species were obtained. Besides the conventional 1:1 fully ionic insulators with segregated stacks, tetramethyl-TTF·CF_3TCNQ·CH_3CN and bis(methylthio)ethylenedithio-TTF·CF_3TCNQ had fully ionic alternating stacks of DDAA units and showed Frenkel triplet excitons. $(BEDO\text{-}TTF)_2(CF_3TCNQ)$ [BEDO-TTF: bis(ethylenedioxy)-TTF] consisted of a mixed-valence segregated stack of donor molecules and completely ionized acceptor molecules, and showed metallic behavior down to 1.8 K even in a compressed pellet sample. Langmuir–Blodgett films composed of $(BEDO\text{-}TTF)_2(CF_3TCNQ)$ and matrix (arachidic acid) showed a conductivity of 3–6 S cm^{-1} at room temperature and a nearly temperature-independent conductivity down to 80 K. Semiconducting $(TMTSF)_2(CF_3TCNQ)$ (TMTSF: tetramethyltetraselenafulvalene) had one-dimensional segregated stacks of dimerized TMTSF molecules separated by completely ionized CF_3TCNQ, the molecular plane of which was arranged parallel to the TMTSF column. The ionicity phase diagram of the CF_3TCNQ CT solids, i.e., a plot of the first CT transition energy vs. donor strength, clearly discriminated these different kinds of CT solids and will be utilized for the prediction and design of the functional CT solids.

Numerous organic functional charge-transfer (CT) solids have been developed based on 7,7,8,8-tetracyanoquinodimethane (TCNQ) and its derivatives, such as metals (e.g., TTF·TCNQ[1]), superconductors (e.g., (BEDT-TSF)(Cl_2TCNQ)[2]), field-effect transistors (FETs),[3] metallic Langmuir–Blodgett (LB) films (e.g., BEDO-TTF·C_{10}TCNQ[4a] and BEDO-TTF·$(MeO)_2$TCNQ[4b]), ferroelectrics by neutral–ionic (N–I) phase transition and order–disorder phenomenon (e.g., 3,3′,5,5′-tetramethylbenzidine·TCNQ,[5a] TTC_1-TTF·2,5-FMe-TCNQ,[5b] and Me_2P·Me_2TCNQ[5c]), condensers,[6] switching and memory systems (e.g., Cu·TCNQ[7a] and $TTeC_1$-TTF·TCNQ[7b,7c]), molecular rectifiers,[8] nonlinear optical materials (e.g., perylene·TCNQ[9] and zwitterionic molecules[10]), and spin-Peierls systems[11] (main molecules discussed in this paper are shown in Scheme 1). For organic electronics such as metals, (super)-conductors and FETs, fine tuning of the Fermi level is crucial,[3,12] and therefore, it is essential to obtain a variety of TCNQ derivatives to cover a wide range of electron-accepting abilities. A trifluoromethyl-TCNQ (CF_3TCNQ) molecule has a stronger electron accepting ability [$E^1_{1/2} = +0.44$ V vs. SCE (saturated calomel electrode)][13] and a lower symmetry than those of TCNQ ($E^1_{1/2} = +0.22$ V vs. SCE). One of the consequences of the use of low symmetric and strong acceptor molecules is that, in general, they can afford dimerized units of the anion radical molecules in order to cancel both net dipole moments and degree of spin freedom and hence form $(D^{\bullet+})_2(A^{\bullet-})_2$ alternating stacks resulting in the formation of

† Present address: Mitsubishi Chemical Corporation
†† Present address: Nissan Arc, Ltd.
††† Present address: Konica Minolta Business Technologies, Inc.
†††† Present address: Photonics Research Institute (PRI), National Institute of Advanced Industrial Science and Technology (AIST)
††††† Present address: Tohoku University
†††††† Present address: Asahi Kasei Corporation

Published on the web December 2, 2010; doi:10.1246/bcsj.20100102

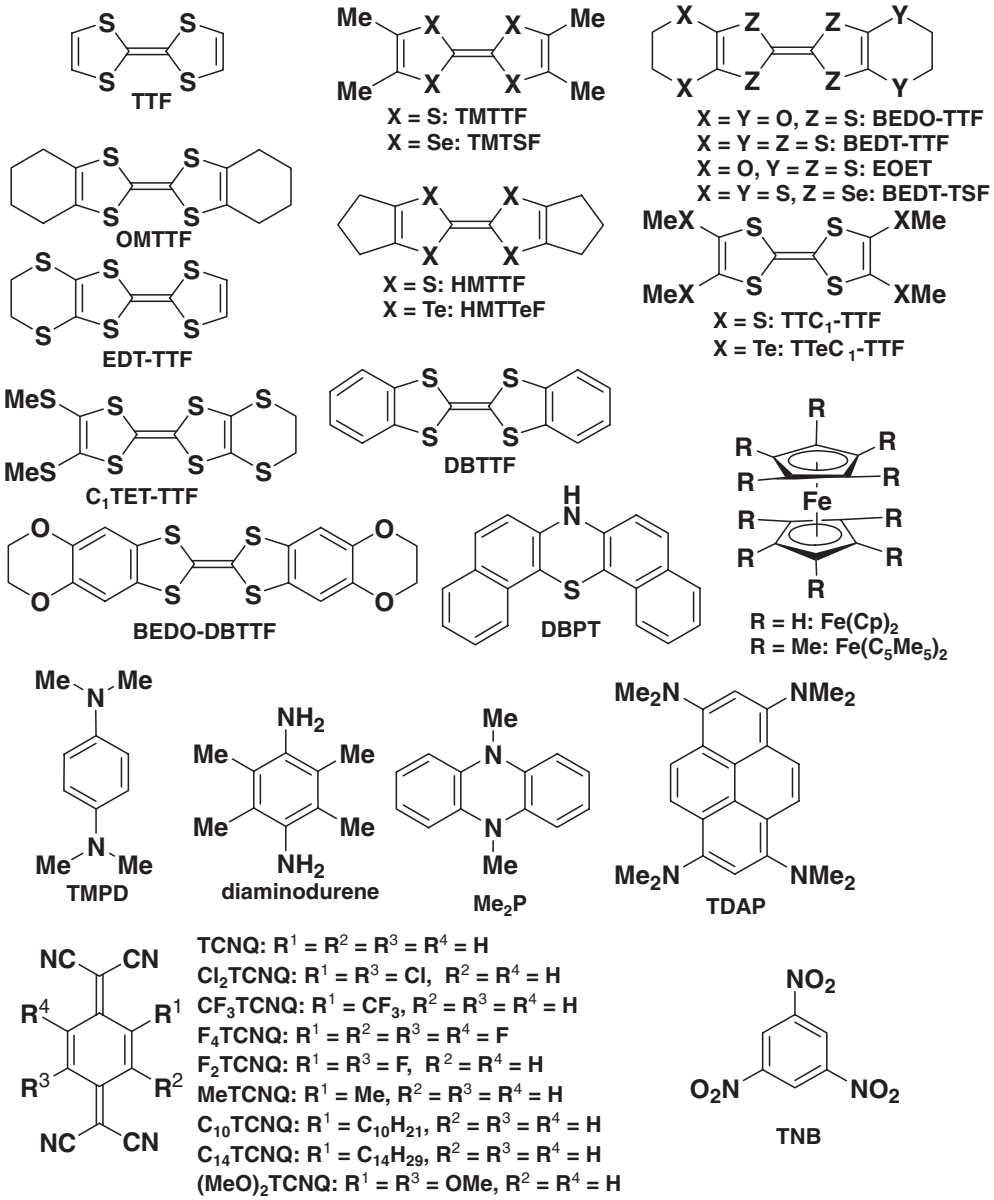

Scheme 1. Main molecules discussed in text.

triplet excitons, where D and A are donor and acceptor molecules, respectively. Another consequence is that they can afford mixed valent cation radical salts $[(D)_n]^+(A^{\bullet-})$ in which $D^{1/n+}$ molecules form segregated assemblies and $A^{\bullet-}$ molecules act as counter anions. Therefore, the low symmetric and strong acceptor CF_3TCNQ afforded amphiphilic conductors $[(D)_n]^+(CF_3TCNQ^{\bullet-})$ which can be transformed into LB films by the aid of hydrophobic CF_3 group. With these properties in mind, we prepared CT solids of CF_3TCNQ with a variety of donor and cation molecules and made an ionicity phase diagram which imparts deep insight into the ionicity, stacking manner, and functionalities.

This paper consists of the following sections to reveal the ionicity diagram of title acceptor molecule after "Experimental" section: "Formation of CT Solids of CF_3TCNQ" overviews the CT complexes, "Ionicity Phase Diagram and Classification of CT Solids" provides the general information to understand the ionicity diagram, "Classification and Characterization of CF_3TCNQ CT Solids" describes the title complexes in the order of our classification, and "Ionicity Diagram for CF_3TCNQ CT Solids" concludes the title phase diagram.

Experimental

All of the components were purified by recrystallization and/or sublimation after preparation in our laboratory or purchased commercially. The optical measurements were performed on a Perkin-Elmer 1600 Series FT-IR spectrometer (resolution 4 cm^{-1}) for the IR and near-IR (NIR) regions (400–7800 cm^{-1}) in KBr, and on a Shimadzu UV-3100 spectrometer for the UV–vis–NIR region (3800–42000 cm^{-1}) in KBr or in solution. The dc conductivities were measured by a standard four- or two-probe technique attaching gold wires (15 $\mu m \phi$) to

Table 1. Stoichiometry, Optical (IR, UV–vis–NIR) and Conductivity Data, and Type (Ionicity and Stacking Mode, See Text) of CF_3TCNQ CT Solids with *Alkali and Onium Ions*

D[a]	D:A:solvent	IR $\nu_{C\equiv N}/cm^{-1}$ (CF_3TCNQ^0: $\nu_0 = 2223\,cm^{-1}$)						UV–vis–NIR/$10^3\,cm^{-1}$			Conductivity	Type[d]
		ν_1	ν_2	ν_3	ν_4	ν_5	ν_6	B′	C′[b]	D′[c]	$\sigma_{RT}/S\,cm^{-1}$	
1 Li	1:1:3/4H_2O	2217	2205	2193	2179		2132	9.7	11.3	15.9	$<10^{-8}$	**IuS**
2 Na	1:1		2208		2180			8.5	11.3	15.4	$<10^{-8}$	**IuS**
3 K	1:1		2201	2191	2178		2137	8.6	11.3	15.9	$<10^{-8}$	**IuS**
4 NH_4	1:1		2202	2193	2179		2137	8.7	11.3	15.7	$<10^{-8}$	**IuS**
5 Rb	1:1		2199	2193	2178		2137	9.5	11.3	15.6	$<10^{-8}$	**IuSn**
6 Cs	1:1			2194	2175		2135	10.5	11.3	15.3	$<10^{-8}$	**IuSn**
7 *N*-MeQ	1:1:1/4H_2O			2190	2181	2166	2125	8.7	11.4	15.6	$<10^{-8}$	**IuSn**

a) *N*-MeQ: *N*-methylquinolinium. b) C (or C′) -band is further classified into C_D, C_2, and C_M-band according to their origins, see text. c) D- and D′-bands are ascribed to intramolecular second HOMO → HOMO transition of cation or donor species and intramolecular LUMO → second LUMO transition of CF_3TCNQ species, respectively. d) See text, to classify the CT solids, ionicity and stacking are labeled as: **I** (fully ionic, $\delta = 1$), **M** (mixed valence, $1 > \delta \geq 0.5$), **M′** (mixed valence, $0.5 > \delta \geq \delta_c$), **N** (neutral, $\delta_c > \delta \geq 0$), **A** (alternating stacks), **A2** (DDAA alternating stacks), and **S** (segregated stacks or layers).

samples with gold paste (Tokuriki 8560-1A). The electron paramagnetic resonance measurements were performed with an EPR X-band spectrometer (JEOL-TE200X). X-ray diffraction data for C_1TET-TTF·CF_3TCNQ (**25**) and TMTTF·CF_3TCNQ·MeCN (**35**) were collected on a CCD diffractometer (Bruker SMART APEX II) with graphite monochromated Mo Kα radiation at 300 K. The empirical absorption correction was carried out using the program SADABS in Bruker APEX2 software by a multi-scan method. The crystal structures were solved by a direct method of SHELXS[14] and refined by full matrix least-squares of F^2 by means of SHELXL.[15] All non-hydrogen atoms were refined anisotropically. The positional parameters of the hydrogen atoms were calculated under a fixed C–H bond length of 1.00 Å with sp^2 or sp^3 configuration of the bonding carbon atoms. In the refinement procedures, isotropic temperature factors with the magnitudes of 1.5 fold for methylene groups and 1.2 times for others to those of the equivalent temperature factors of the bonding carbon atoms were applied for hydrogen atoms. Crystallographic data have been deposited with Cambridge Crystallographic Data Centre: Deposition numbers CCDC-767692 for **25** and CCDC-767693 for **35**. Copies of the data can be obtained free of charge via http://www.ccdc.cam.ac.uk/conts/retrieving.html (or from the Cambridge Crystallographic Data Centre, 12, Union Road, Cambridge, CB2 1EZ, U.K.; Fax: +44 1223 336033; e-mail: deposit@ccdc.cam.ac.uk). A conventional Langmuir trough (LAUDA film balance) was used for the deposition of multilayers. X-Type LB films were deposited by horizontal lifting. The arachidic acid was added as a matrix molecule to increase the quality of LB films.

Formation of CT Solids of CF_3TCNQ

A variety of organic and inorganic species afforded CT solids with CF_3TCNQ. The considerably high solubility of CF_3TCNQ in conventional organic solvents, e.g., 0.1 g mL^{-1} in acetonitrile (MeCN), rendered difficult the isolation of CT solids. This propensity may be caused by the low-symmetry and highly polarizable nature of CF_3TCNQ. Tables 1–3 summarize the donor molecules used, stoichiometry determined by elemental analyses (see Supporting Information: Table S1), multiple C≡N stretching frequencies ($\nu_{C\equiv N}$: ν_1–ν_6 in the order of frequency), UV–vis–NIR absorption energies for bands A–D ascribable to donor molecules and bands B′–D′ ascribable to the acceptor molecule, room-temperature (RT) conductivity (σ_{RT}), and the activation energy (ε_a) of conduction for the CT solids with alkali metals and ammonium derivatives (Table 1), aromatic hydrocarbons, amines, and azines (Table 2), and TTF derivatives (Table 3). The donor molecules (D) in Tables 2 and 3 are arranged according to the donor strength evaluated from the CT transition energies of the *s*-trinitrobenzene (TNB) complexes ($h\nu_{CT}$(D·TNB) in $CHCl_3$), which are presented in brackets in the first column. CT solids **1**, **7**, **10**, **13**–**18**, **21**, **22**, **26**, **30**–**32**, and **34**–**36** include solvent molecules during crystallization. It is notable that many kinds of TTF derivatives produced more than one modifications of complexes with CF_3TCNQ showing different physical and/or structural properties; **21**–**24**, **30** and **31**, **32** and **33**, and **35** and **36**.

The ionicity of CT solids (δ) was estimated mainly by IR and UV–vis–NIR spectra, with the aid of electrical conductivity, magnetic properties, and stoichiometries of the solids as has been done in other CT systems[16] based on TTF derivatives,[16b,16d–16f,16k–16m,16r] aromatic amines,[16a,16c,16g,16n] C_{60},[16h] 2,2′-biimidazole,[16i,16j] and a few proton donors.[16a,16p] The analyses provided molecular packing pattern information even without crystal structure analysis by diffraction methods. In the last column of Tables 1–3, the classification of the CT solids based on their ionicity and stacking mode is summarized. Such classification is one of the most essential strategies for exploration of functional CT solids and has been elucidated by several researchers.[17–19]

The ionicity is classified into fully ionic ($\delta = 1$, **I**), mixed valence ($1 > \delta \gg 0$; in this paper, the ionicity of $1 > \delta \geq 0.5$ is represented by **M** and that of $0.5 > \delta \geq \delta_c$ by **M′**), and neutral ($\delta_c > \delta \geq 0$, **N**), where δ_c is the critical degree of ionicity for mixed valence that depends on the electronic dimensionality ($\delta_c = 0.5$ for one-dimensional TTF·TCNQ system and $0.5 > \delta_c > 0$ for 2- and 3-dimensional conductors). Since the CF_3TCNQ molecules in CT solids tend to be fully ionized (vide infra), the symbols for ionicity in Tables 2 and 3 are derived from the donor component. The alternating and segregated stacks are denoted as **A** and **S**, respectively. When the uniform

Table 2. Stoichiometry, Optical (IR, UV–vis–NIR) and Conductivity Data, and Type (Ionicity and Stacking Mode, See Text) of CF_3TCNQ CT Solids with *Aromatic Hydrocarbons, Amines and Azines*

D[a] [$h\nu_{CT}/10^3\,cm^{-1}$]	D:A:solvent[b]	IR $\nu_{C\equiv N}/cm^{-1}$						UV–vis–NIR/$10^3\,cm^{-1}$					Conductivity		Type[e]
		ν_1	ν_2	ν_3	ν_4	ν_5	ν_6	$h\nu_{CT}^N$	A	B′	C′[c] (C[c])	D′[d] (D[d])	σ_{RT} /S cm^{-1}	ε_a /meV	
8 triphenylene [27.5]	1:1	2220						16.6					$<10^{-8}$		**NuA**
9 pyrene [22.2]	1:1	2220						12.3					$<10^{-8}$		**NuA**
10 HMTP [21.0]	1:1:4/3$CHCl_3$	2217						9.7					$<10^{-8}$		**NuA**
11 perylene [20.8]	1:1	2218						9.0					$<10^{-8}$		**NuA**
12 PT [19.0]	1:1	2212						6.7					$<10^{-8}$		**NuA**
13 DBPT [17.4]	1:1:3/5PhMe				2175		2126			10.0	11.3	14.8	$<10^{-8}$		**IuSn**
14 diaminodurene [17.1]	1:1:1/2PhH		2200	2185							11.6	14.4	$<10^{-8}$		**IuA2**
15 $Fe(Cp)_2$ [16.0]	6:5:2MeCN			2189	2180	2166			3.3	9.2	11.3	15.9	3.6×10^{-1}	52	**MS**
16 TMPD [15.7]	1:1:1/2PhH			2187			2136			9.8	11.5 (13.4)	14.6 (15.3)	$<10^{-8}$		**IuSn**
17 Me_2P [14.2]	1:1:1/3PhH			2189		2162				9.2	11.3	15.3	$<10^{-8}$		**IuSn**
18 TDAP [14.0]	1:2:1H_2O			2184		2163				8.5	11.3 (12.8)	13.9	$<10^{-8}$		**IuS** or **IuA**
19 $Fe(C_5Me_5)_2$ [13.8]	1:1			2187		2169				10.5	11.3	14.2	$<10^{-8}$		**IuSn**

a) PT: phenothiazine, HMTP: hexamethoxytriphenylene. For other abbreviations of donors, see Scheme 1. b) PhH: benzene, PhMe: toluene. c) C (or C′)-band is further classified into C_D, C_2, and C_M-band according to their origins, see text. d) D- and D′-bands are ascribed to intramolecular second HOMO → HOMO transition of cation or donor species and intramolecular LUMO → second LUMO transition of CF_3TCNQ species, respectively. e) See text, to classify the CT solids, ionicity and stacking are labeled as: **I** (fully ionic, $\delta = 1$), **M** (mixed valence, $1 > \delta \geq 0.5$), **M′** (mixed valence, $0.5 > \delta \geq \delta_c$), **N** (neutral, $\delta_c > \delta \geq 0$), **A** (alternating stacks), **A2** (DDAA alternating stacks), and **S** (segregated stacks or layers).

Table 3. Stoichiometry, Optical (IR, UV–vis–NIR) and Conductivity Data, and Type (Ionicity and Stacking Mode, See Text) of CF_3TCNQ CT Solids with *TTF Derivatives*

D[a] [$h\nu_{CT}/10^3\,cm^{-1}$]	D:A:solvent[b]	IR $\nu_{C\equiv N}/cm^{-1}$					UV–vis–NIR/$10^3\,cm^{-1}$							Conductivity		Type[e]
		ν_1	ν_2	ν_3	ν_4	ν_5	A	B′	B	C′[c]	C[c]	D′[d]	D[d]	σ_{RT} /S cm^{-1}	ε_a /meV	
20 DBTTF [17.3]	3:2	2205	2198				$h\nu_{CT}^N = 6.8, 17.1$							$<10^{-8}$		**NuA**
21 BEDT-TTF [16.1]	5:3:1PhCl			2186	2179	2163	3.4			10.3		15.7	10.3	3.0×10^{-2}	68	**MS**
22	5:3:4/3PhCN			2186	2178	2166	2.9			10.2		15.9	10.2	1.4	58	**MS**
23[f]	5:3 (CS_2)			2184		2168	3.3			11.2		15.5	11.2	2.0	57	**MS**
24[f]	2:1 (TCE)			2188		2163	3.1	7.7		11.0		15.1	11.0	4.2	32	**MS**
25 C_1TET-TTF [16.0]	1:1			2185		2164				10.8		14.3		1.0×10^{-6}	282[h]	**IuA2**
26 BEDO-DBTTF [15.8]	2:1:1/3PhCl			2189		2166	3.3	8.3		11.5		14.2	13.2	3.3×10^{-1}	92	**MS**
27 HMTTeF [15.8]	4:3	2206		2185		2162	ca. 3	5–8		11.5		14.1	12.9	4.1	32	**MS**
28 EDT-TTF [15.7]	2:1			2188	2180	2165	4.7	8.6		11.5		14.5	13.3	4.4×10^{-3}	156	**MS**
29 EOET [15.5]	ca.2:1			2185		2165	3.6	7.3		11.3		15.1	11.3	5.8	metal >252 K	**MuS**
30 TTF [15.4]	10:9:4THF			2189		2169	4.1	8–10		11.3	12.9	15.7	19.3	1.0	140	**MSn**
31	1:1:2/3PhMe			2193	2183	2169		8.2	9.8	11.3		15.7	19.4	1.5×10^{-6}	181	**IuSn**
32[g] TMTSF [15.0]	1:1:1/2PhCl				2180	2164		8.5		11.5		15.1	13.1	1.2×10^{-5}	354	**IuSn**
33[f]	2:1 (PhCl)				2181		2.6			11.5		14.4		5.0×10^{-1}	100[h]	**MuSn**
34 BEDO-TTF [15.0]	2:1:1/2H_2O			2190		2171	2.8	7.2		11.6		14.9	13.3	1.7×10^{2}	metal >1.8 K	**MuSn**
35 TMTTF [13.9]	1:1:1MeCN			2185		2166				11.3	12.8	14.1	17.2	$<10^{-8}$ [h]		**IuA2**
36	1:1:1/4PhMe			2186		2167				11.5	12.8	13.8	16.8			**IuA2**
37 OMTTF [13.8]	1:1				2181	2159				11.1	12.6	15.3		$<10^{-8}$		**IuA2**
38 HMTTF [13.7]	1:1			2186		2164				11.3	12.6	14.8	16.0	$<10^{-7}$		**IuA2**

a) Abbreviations of donors, see Scheme 1. b) PhMe: toluene, PhCl: chlorobenzene, PhCN: benzonitrile, TCE: 1,1,2-trichloroethane, THF: tetrahydrofuran. c) C (or C′)-band is further classified into C_D, C_2, and C_M-band according to their origins, see text. d) D- and D′-bands are ascribed to intramolecular second HOMO → HOMO transition of cation or donor species and intramolecular LUMO → second LUMO transition of CF_3TCNQ species, respectively. e) See text, to classify the CT solids, ionicity and stacking are labeled as: **I** (fully ionic, $\delta = 1$), **M** (mixed valence, $1 > \delta \geq 0.5$), **M′** (mixed valence, $0.5 > \delta \geq \delta_c$), **N** (neutral, $\delta_c > \delta \geq 0$), **A** (alternating stacks), **A2** (DDAA alternating stacks), and **S** (segregated stacks or layers). f) **23**, **24**, and **33** were prepared from CS_2, TCE, and PhCl, respectively, without solvent inclusion. g) Contaminated with **33**. h) Data on single crystals.

ionicity and/or stacking manner are confirmed, a small character of **u** is added (**n** for non-uniformity). For example, a 2:1 solid with $\delta = 0.5$ and a dimerized segregated stack is labeled as **MuSn**.

Ionicity Phase Diagram and Classification of CT Solids

Precautions Making Ionicity Phase Diagram. Several classifications of CT solids have been proposed to understand their perspectives.[17–19] However, all earlier studies[17] were incomplete for understanding the whole picture of CT solids, since they lacked 1) neutral segregated stacks (Type **NS**),[5d,16h,20,21] 2) metallic alternating stacks (Type **MnAu**),[16m] 3) metallic segregated layers with charge disproportionation (Type **MnSu**),[22] and 4) 1:1 metallic segregated stacks with fully ionized CT solids (Type **ISu**) composed of molecules of small on-site Coulomb repulsive energy (U).[23]

One has to seek an appropriate DA combination to have appropriate ranges of $I_P - E_A$ (I_p: ionization potential of an electron donor molecule, E_A: electron affinity of an electron acceptor molecule), which can be conventionally replaced by the solution redox difference $\Delta E(\mathrm{DA}) = E_1(\mathrm{D}) - E_1(\mathrm{A})$ (E_1: first redox potential) to obtain particular functional materials, e.g., organic metals with mixed valence states. Besides that, it is strongly recommended to include component molecules with similar sizes and shapes for an ionicity phase diagram[16a,24] to have common Madelung energy (M), self-assembling ability, and dimensionality in a particular DA system. Otherwise, for example, the combination with the components with very different size needs careful examination concerning these parameters to obtain correct information for the functionalities.

Ionicity Phase Diagram and Its Utility. Figure 1 shows the relationship between two kinds of ionicity phase diagrams.[16b,25] Figure 1a is a plot of electrical conductivity data of 1:1 low-dimensional TTF·TCNQ system, vs. redox potentials. The component molecules have weak self-assembling ability but sufficient to form segregated stacks. The basic concept of this figure is derived from similar plots for CT solids of aromatic diamine systems,[16a,24] where the much weaker self-assembling ability of the constituents results in non-segregated but mainly alternating stacks, and therefore, the correlation between the conductivity and ionicity was not clear.

The two lines **a** and **b** in Figure 1a are related to the equation expressing the relationship among I_P, E_A, and the Madelung energy $M(\delta)$ between partially charged component molecules (eq 1).[26] The mixed valence region (**M**) is located between fully ionic (**I**) and neutral (**N**) regions. In the region **M**, the CT solids are either highly conductive (○) or metallic (●) when they have segregated stacks. The solids in the regions **I** and **N** are insulators (△), in general.

$$I_P - E_A = M(\delta) \tag{1}$$

Figure 1a was made by rotating the original figure in Ref. 16b so as to have two borderlines **a** and **b** vertical. Then, every CT solid allocated on the horizontal line in Figure 1a has the same chemical potential ($I_P + E_A = \text{constant}$).[27] As an application of this diagram, the organic metals in the region **M** residing on the varied horizontal lines in Figure 1a were employed as the source and drain electrodes to control the

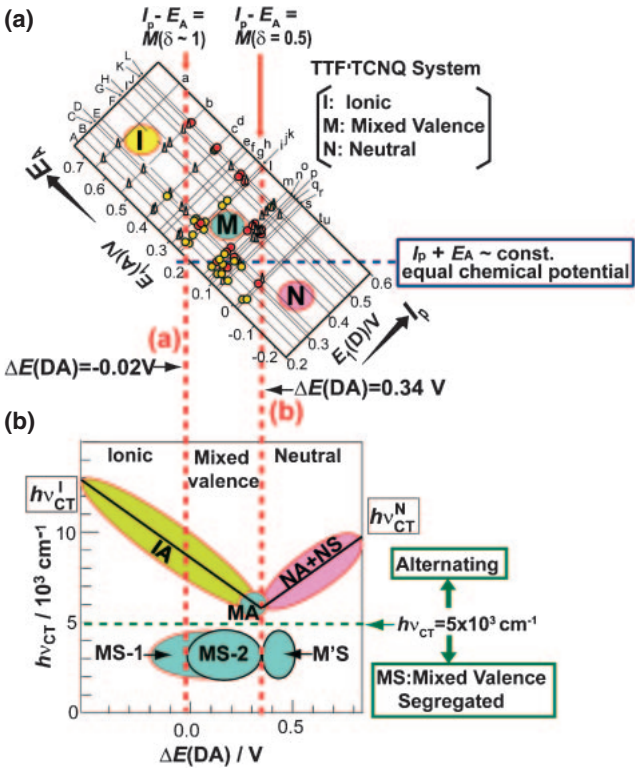

Figure 1. (a) Ionicity diagram for TTF·TCNQ system plotted as E_1(A) vs. E_1(D) after modification of the original diagram in Ref. 16b. Open triangle: insulators or semiconductors; yellow circle: highly conducting in compaction studies; red circle: organic metals. The representative components are A: tetrathionaphthacene, B: TMTTF, D: TTF, E: HMTTF, F: HMTSF, G: TMTSF, H: TSF, J: TTC_1-TTF, K: BEDT-TTF, L: DBTTF, a: 2,5-$(CN)_2$TCNQ, b: F_4TCNQ, e: 2,5-I_2TCNQ, f: F_2TCNQ, i: FTCNQ, m: TCNQ, n: MeTCNQ, p: 2,5-Et_2TCNQ. E_1(A) and E_1(D) in this figure are the peak values vs. SCE. Region N: neutral, M: mixed valence, I: fully ionic. Line a: $\Delta E(\mathrm{DA}) = -0.02$ V, b: $\Delta E(\mathrm{DA}) = 0.34$ V. Organic metals on the blue dotted line have the same chemical potential ($I_p + E_A = \text{constant}$). (b) Schematic phase diagram of ionicity, conductivity and stacking of DA CT solids. The first transition energy in solid ($h\nu_{CT}$) is plotted against the ΔE(DA) value. Left- and right-hand sides of the V-shaped line correspond to eqs 2 and 3, respectively. IA: ionic alternating, MA: mixed-valence alternating, NA: neutral alternating, NS: neutral segregated, MS: mixed-valence segregated (**MS-1**: non 1:1 (one component is fully ionic), **MS-2**: 1:1 low-dimensional, **M′S**: 1:1 high-dimensional). An appropriate V-shaped line for the TCNQ system was obtained by a parallel shift of the V-shaped line for the *p*-quinone system toward the lower side by 0.13–0.16 V.

Fermi level alignment between electrodes and channel for FETs making the injection of carriers smooth and giving varied FET polarity.[3]

Figure 1b is based on the CT transition energies of neutral ($h\nu_{CT}^{N}$, eq 2) and ionic ($h\nu_{CT}^{I}$, eq 3) solids instead of conductivity, to discriminate between the neutral and ionic solids with alternating stacks (V-shaped line in Figure 1b),[25] and therefore this ionicity phase diagram can be made more readily

than Figure 1a since the conductivity measurements are time consuming.

$$h\nu_{CT}{}^{N} = I_P - E_A - C \quad (2)$$

$$h\nu_{CT}{}^{I} = -I_P + E_A + (2\alpha - 1)C \quad (3)$$

where C and αC are the Coulomb attractive energy between $D^{\bullet+}$ and $A^{\bullet-}$ and the Madelung energy, respectively. The N–I phase boundary condition ($h\nu_{CT}{}^{N} = h\nu_{CT}{}^{I}$) gives the same criterion as eq 1. In the neutral region near the bottom of the V-shaped line, an enantiotropic phase transition system (N–I transition) is allocated, since the contraction by lowering temperature favors ionic species by enhancing M.[25a]

The CT solids that have $h\nu_{CT}$ bands below $5 \times 10^3\,cm^{-1}$ (horizontal green dotted line) belong to a different class (region **MS**) from those residing on the V-shaped line. Region **MS** that usually includes (super)conductors[12,16k–16m,16q,18,28–31] and narrow-gap semiconductors has mixed valence segregated stacks or layers.

Among the region **MS**, **MS-1** is for non 1:1 CT solids in which the minor component is fully ionized and thus the major one has a mixed valence state.[2,32,33] **MS-2** is for low-dimensional 1:1 CT solids in which both component molecules are in mixed-valence states.[16b,16q] When highly conductive 1:1 CT solids are located in this region exclusively, it is safely concluded that the system has a low-dimensional electronic structure.[16b,16q] **M′S** is for high-dimensional 1:1 CT solids, which usually extend their metallic regime toward lower δ values (higher ΔE(DA) values) like the HMTTeF[16m,16o] and BEDO-TTF[16k] systems owing to their strong self-assembling ability. Even with $\delta = 1/3$, some BEDO-TTF complexes have segregated stack and show metallic behavior.[16k,34]

Figure 1 gives us a prediction on the modes of molecular stacking: **A** and **S**, and information on the chemical potentials and other functionalities as described below.

Near the borderline **b** in Figure 1a, the bistability concerning the ionicity between the neutral and partial CT states is realized, i.e., the monotropic complex isomers G·m,[35] H·p,[36] and K·m.[16b,16c,37] Even though K·m (BEDT-TTF·TCNQ) is expected to afford a neutral insulator based on its ΔE(DA) value, a highly conductive complex isomer has been prepared.[37a] This indicates that the BEDT-TTF molecule has a significant self-assembling ability to form a segregated column with increased dimensionality, which is the nature of the solids in the region **M′S** in Figure 1b and leads to the formation of 2-dimensional conductors and superconductors.[12,18,38] The insulating CT solids residing near the borderline **a** or **b** have the potential to exhibit a phase transition into a highly conducting phase induced by external stimuli (electric field, photo, etc.) with smaller threshold than those allocating far from the borderlines.[7b,39]

The fully ionic solids (region **I**) afforded band insulators, 1:1 Mott insulators with ground states of antiferromagnets (E·b and F·b)[40] or spin-Peierls,[11,41] ferroelectrics,[42] ferromagnets,[43] spin-ladders,[44] and nonlinear transport materials (switching and memory).[7,39]

The mixed valence (region **M** in Figure 1a, and **MA**, **MS-1**, **MS-2**, and **M′S** in Figure 1b) afforded (super)conductors and the following various insulators: 1) a (nearly) uniform segregated stack having spin density wave, and anion or charge ordered (=charge disproportionation) state,[11a,18,29,45] 2) a non-uniform segregated stack showing Peierls-type distortion,[28,29] spin-Peierls distortion,[11,46] and dimer-type Mott insulators[18] including antiferromagnets,[47] spin-liquid[48] and spin-ladders,[49] and 3) an alternating stack including N–I systems, ferroelectrics,[50] and highly-conductive semiconductors.[16m,51] There are hybrids by the combination of ferro-, ferri-, or paramagnetic species based on transition-metal compound as one component and mixed valence counterpart to form magnetic CT conductors.[52]

The neutral solids (**N** and **NA** + **NS**), in general, exhibit a CT band represented by eq 2 regardless of the stacking modes.[16h,20b] Since most CT solids in the region **N** prefer alternating stacks with a few exceptions,[5d,16h,20a,21,53b,53c] they are band insulators with low ionicity. Hydrogen bond and proton transfer between the components manifest many interesting functions; switching, ferroelectrics, etc.[53]

Figure 1b does not include fully ionic CT solids of both Type **IS** and Type **IA2** (alternating stack of fully ionic dimerized D and A: $D^+D^+A^-A^-$) since they exhibit CT bands with different energies and will be described below.

Classification of CT Solids by Optical Bands $h\nu_{CT}{}^{N}$, $h\nu_{CT}{}^{I}$, and A–C. Here we briefly describe the relationship between the optical bands measured on a KBr disk in the UV–vis–NIR and IR regions ($h\nu_{CT}{}^{N}$, $h\nu_{CT}{}^{I}$, A–D, A′–D′-bands), and ionicity and stacking modes of the CT solids. The details are described in Ref. 19.

$h\nu_{CT}{}^{N}$ and $h\nu_{CT}{}^{I}$: For alternating stacks, the solids exhibit either $h\nu_{CT}{}^{N}$ for Type **NA** or $h\nu_{CT}{}^{I}$ for Types **IA** and **MA**. Segregated neutral solids (Type **NS**) also exhibit CT bands expressed by eq 2. In some solids of Type **IA**, however, an optical transition between $D^{\bullet+}$ or $A^{\bullet-}$ species (B- or B′-band, respectively, eq 4) appears and there is no back CT transition ($h\nu_{CT}{}^{I}$) from $A^{\bullet-}$ to $D^{\bullet+}$.[54]

$$\underset{\text{B-band}}{\overset{\curvearrowright}{\mathbf{D^{\bullet+}D^{\bullet+}D^{\bullet+}D^{\bullet+}}}} \rightarrow \mathbf{D^{\bullet+}D^{2+}D^{0}D^{\bullet+}}; \quad \underset{\text{B'-band}}{\overset{\curvearrowright}{\mathbf{A^{\bullet-}A^{\bullet-}A^{\bullet-}A^{\bullet-}}}} \rightarrow \mathbf{A^{\bullet-}A^{0}A^{2-}A^{\bullet-}} \quad (4)$$

B-Band: Except for the above-mentioned case, the appearance of B- (B′-) band is a typical phenomenon for solids with segregated stacks with $\delta \geq 0.5$ (Type **IS**, **MS**). The intensity of B-band decreases with decreasing ionicity and becomes nearly zero-intensity at $\delta = 0.5$.[55] It is easy to discriminate between Types **IS** and **MS**, since the latter exhibits additional low-energy band below $5 \times 10^3\,cm^{-1}$ (A-band). The B- (B′-) band usually appears at 5–13 $\times$ $10^3\,cm^{-1}$ for TTF and TCNQ systems in solids and disappears in dilute solutions.

C-Band: In the case of fully ionic and non-uniform segregated column (Type **ISn**), an extra band appears at higher energy than the B-band. For a dimerized system, intra- and interdimer bands are observed as B- (B′-) and C_D- (C_D′-) bands (D denotes distortion), respectively (eq 5).

$$\underset{\text{B-band}}{\overset{\curvearrowright}{\mathbf{D^{\bullet+}D^{\bullet+}}}}\mathbf{D^{\bullet+}D^{\bullet+}}; \quad \underset{\text{B'-band}}{\overset{\curvearrowright}{\mathbf{A^{\bullet-}A^{\bullet-}}}}\mathbf{A^{\bullet-}A^{\bullet-}} \quad (5)$$

$$\underset{C_D\text{-band}}{\overset{\curvearrowright}{\mathbf{D^{\bullet+}D^{\bullet+}}}} \qquad \underset{C_D\text{'-band}}{\overset{\curvearrowright}{\mathbf{A^{\bullet-}A^{\bullet-}}}}$$

The C_D'-band appears at around $11 \times 10^3\,cm^{-1}$ for the TCNQ system. Since the C_D- (C_D'-) band grows rapidly with lattice distortion, it can be used as an index for lattice distortion provided the simultaneous appearance of IR inactive a_g mode in the IR spectrum. When a solid contains isolated radical molecules of TCNQ derivatives, it shows a sharp peak with fine structures, labeled as C_M'-band (M denotes monomer), in the $10–11 \times 10^3\,cm^{-1}$ region, similar to that of radical anions in solution. C_M'-band also appears weakly for metallic solids with uniform segregated columns on the compressed KBr pellet measurement.

Several fully ionic complexes with DDAA stack are known (Type **IA2**, where **2** stands for dimerized unit).[56a–56l] They show characteristic optical bands (C_2- or C_2'-band) ascribable to the optical process eq 6, but no $h\nu_{CT}^{I}$ (CT transition from $A^{\bullet-}$ to $D^{\bullet+}$) usually.

$$\underset{\text{C}_2\text{-band}}{\mathrm{D^{\bullet+}D^{\bullet+}A^{\bullet-}A^{\bullet-}} \rightarrow \mathrm{D^{2+}D^{0}A^{\bullet-}A^{\bullet-}};} \qquad \underset{\text{C}_2\text{'-band}}{\mathrm{D^{\bullet+}D^{\bullet+}A^{\bullet-}A^{\bullet-}} \rightarrow \mathrm{D^{\bullet+}D^{\bullet+}A^{0}A^{2-}}} \tag{6}$$

The C_2- (or C_2'-) band appears at higher energy than the B- (or B′-) band.

A-Band: In the IR region, ionic and neutral complexes show the vibrational absorption spectra of component ions (molecules). In the case of metallic solids, however, these bands are difficult to observe due to the intraband transition, which appears below $5 \times 10^3\,cm^{-1}$ on KBr pellet measurements (A- or A′-band). A CT band below $5 \times 10^3\,cm^{-1}$ is also observed for narrow gap semiconductors and assigned as A- or A′-band since it is indistinguishable from the band of metallic solids on KBr pellet measurements. The optical band arises from the following process for charge-ordered CT solids.

$$\underset{\text{A-band}}{\mathrm{D^{\bullet+}D^{0}D^{\bullet+}D^{0}} \rightarrow \mathrm{D^{\bullet+}D^{\bullet+}D^{0}D^{0}}} \qquad \underset{\text{A'-band}}{\mathrm{A^{\bullet-}A^{0}A^{\bullet-}A^{0}} \rightarrow \mathrm{A^{0}A^{\bullet-}A^{\bullet-}A^{0}}} \tag{7}$$

Classification and Characterization of CF_3TCNQ CT Solids

Essentially Neutral CT Solid (Type NA). Solids **8–12** and **20** belong to this group, since 1) the IR spectrum of the solid is explained by the superimposition of spectra of neutral component molecules, and 2) their CT absorption bands follow eq 2. Only one C≡N stretching band, which shifts to lower frequency as the donor ability increases ($\nu_1 = 2220–2212\,cm^{-1}$), was observed except the DBTTF complex **20**. For **20**, the CT band ($6.8 \times 10^3\,cm^{-1}$) and C≡N stretching bands ($\nu_1 = 2205\,cm^{-1}$, $\nu_2 = 2198\,cm^{-1}$) suggest that the solid is much closer to the N–I boundary in comparison with those of other complexes of Type **NA**. All of these solids have most likely alternating stacks, since a neutral solid with segregated stacks is rare and usually they are far from 1:1 stoichiometry.[20] They have a σ_{RT} less than $10^{-8}\,S\,cm^{-1}$.

1:1 Fully Ionic CT Solid with Segregated or Self-Assembled Stack (Type IS). Solids **1–7**, **13**, **16–19**, **31**, and **32** belong to this group. Both the strong electron-donating ability of the donor species and the 1:1 or 1:1:*x*(solvent) stoichiometry are responsible for the fully ionic nature of $D^+ \cdot CF_3TCNQ^{\bullet-}$ ($D^{\bullet+}$ when D^0 has a closed shell electronic structure). All the solids in this group, except the TDAP complex **18** with a ratio of 1:2:H_2O which will be described below, were assigned based on UV–vis–NIR and IR spectra as follows.

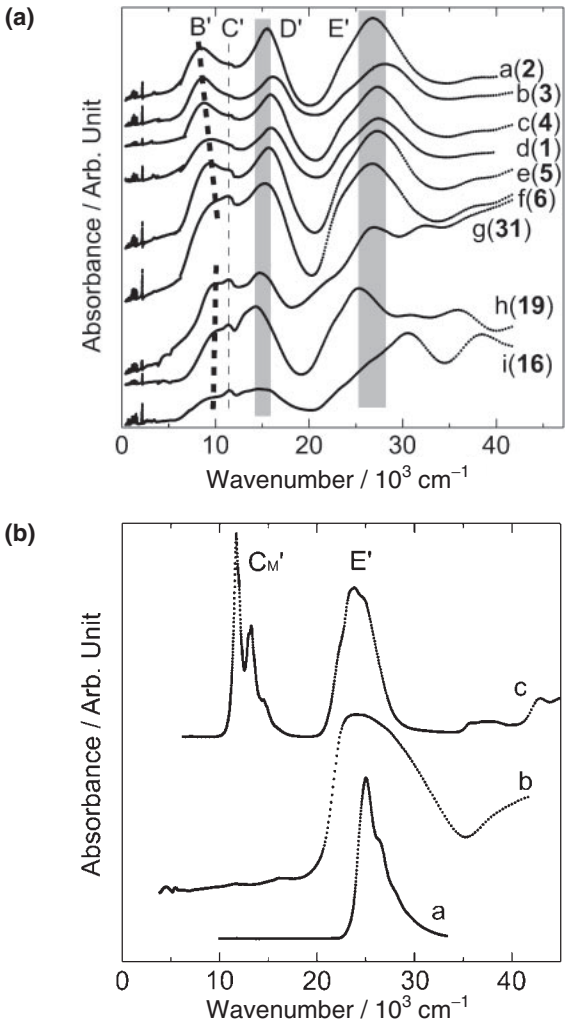

Figure 2. Optical absorption spectra of (a) 1:1 CF_3TCNQ complexes in KBr, with a) Na (**2**), b) K (**3**), c) NH_4 (**4**), d) Li (**1**), e) Rb (**5**), f) Cs (**6**), g) TTF (**33**), h) $Fe(C_5Me_5)_2$ (**19**), and i) TMPD (**16**), and (b) a) CF_3TCNQ in MeCN, b) CF_3TCNQ in KBr and c) $K \cdot CF_3TCNQ$ in MeCN. C_M'-, D′-, and E′-bands are intramolecular transitions of $CF_3TCNQ^{\bullet-}$. The first transition in neutral CF_3TCNQ is close to E′-band of $CF_3TCNQ^{\bullet-}$. For bands B′ and C′, see text. The dotted and thick lines in Figure 2a are guides.

UV–vis–NIR Spectroscopy: In Figure 2, the UV–vis–NIR spectra of several fully ionic solids (Figure 2a) are compared with those of neutral CF_3TCNQ in MeCN and in KBr, and $K \cdot CF_3TCNQ$ in MeCN (Figure 2b). The alkaline and ammonium salts **1–6** show B′- and C′-bands at $8.5–10.5 \times 10^3$ and $11.3–11.5 \times 10^3\,cm^{-1}$, respectively. The B′-band tends to locate at higher energy as the size of D^+ increases, as shown by a thick dotted line. Since the energy of the B′-band is approximated as $h\nu_{CT}(B'\text{-band}) \approx (U - V)/2 + [(U - V)^2/4 + 4t^2]^{1/2} - 2t$,[57] this is most likely caused by the increase of the interplanar distance between $CF_3TCNQ^{\bullet-}$ molecules resulting in the decrease of both transfer interaction, *t*, and nearest site

Table 4. The Vibrational Bands of Some CF_3TCNQ Complexes in the Region of 1600–400 cm^{-1} (Powdered Sample in KBr, See Also Figure 12 for **1**, **24**, **29**, **33**, and **34**)[a)]

Li **1**	TTF[b)] **31**	TMTTF[c)] **35**	BEDT-TTF[d)] **24**	EOET **29**	BEDO-TTF[e)] **34**	TMTSF[c)] **33**
1590	1590	1595	1586 $a\nu_3$	1590	1596 $a_g\nu_2$	1590 $a_g\nu_3$
		1545 $a_g\nu_3$				
1504	1501	1497	1502	1500		1500
1464	1463	1460				
						1436
		1373 MeCN	1408			
1370	1371 $a_g\nu_3$					1390
1352	1356 $a_g\nu_3$	1356 $a_g\nu_4$	1356 $a\nu_5$	1356		
	1338 $a_g\nu_3$					
			1300 $a\nu_4$ (broad)	1300 (broad)	1300 $a_g\nu_3$ (broad)	1290 $a_g\nu_4$
1286	1284	1286				
1266	1266	1266				
1200	1194	1192		1182	1182 $a_g\nu_6$	
			1160 $a\nu_7$			
1168	1166	1170				
1130	1117	1122	1124	1128	1130	1132
1054	1054	1054				
1016	1014	1012	1011 $a\nu_8$	1004	1004 $a_g\nu_7$	
		931 $a_g\nu_8$				908 $a_g\nu_8$
898	895	900				894
			880 $a\nu_{10}$			
				856	858 $a_g\nu_8$	
820	813	814	819			818
	730 PhMe	756 MeCN				
716	714	714	710			
	684 $a_g\nu_5$					
				586	590 $a_g\nu_{10}$	
518	516	504 $a_g\nu_{10}$				520
	484 $a_g\nu_6$		464 $a\nu_{12}$	458		442 $a_g\nu_9$

a) The assignments for the bands assignable to the donor molecules are given according to the symmetry and mode number in references. b) Ref. 58. c) Ref. 59. d) Refs. 60 and 61. e) Ref. 62.

Coulomb repulsion energy, *V*. The appearance of the B′-band at high energy in **1** (9.7×10^3 cm^{-1}) may indicate that the water molecules included in the crystal effectively expand the interplanar distance between $CF_3TCNQ^{\bullet-}$ molecules.

A weak band at around 11×10^3 cm^{-1} is ascribed to the acceptor species (C′-band). The bands have a different shape from the C_M′-band. The C′-band is very weakly observed in **2**–**4** and faintly in **1**, and the type of counterpart makes little impact on the energy of the band (see thin dotted line). The weak C′-band in **1**–**4** is indicative of a very weak dimerization in the $CF_3TCNQ^{\bullet-}$ segregated columns (C_D′-band), if any. With increasing cation size, **5** and **6** exhibited a rather strong C′-band implying that the lattice distortion exists definitely in the $CF_3TCNQ^{\bullet-}$ segregated columns. The similarity of the UV–vis–NIR spectrum of **7** to those of **5** and **6** supports the fully ionic and distorted segregated nature of the $CF_3TCNQ^{\bullet-}$ columns. The strong donor molecules, such as those in **13**, **16**, **17**, **19**, **31**, and **32**, also afforded complexes of D:A = 1:1, which exhibited B′-, C_D′-, D′-, and E′-bands (D′- and E′-bands are intramolecular transitions of $CF_3TCNQ^{\bullet-}$) in addition to the bands originating from the $D^{\bullet+}$ species. This confirms that these solids consist of $D^{\bullet+}$ and $A^{\bullet-}$ species and have distorted segregated stacks of $A^{\bullet-}$. The relative intensity of C′- to B′-bands is markedly enhanced in these solids compared with those in **1**–**4**. This behavior is well interpreted by the increase of distortion in CF_3TCNQ stacks with increasing the cation size.

IR Spectroscopy: Table 4 summarizes the vibrational bands and the assignments for the donor species for some CF_3TCNQ salts in the region of 1600–400 cm^{-1}. In addition to the peaks assignable to the $CF_3TCNQ^{\bullet-}$ species, the IR spectrum of TTF complex **31** exhibited an intense broad band with peaks at 1371, 1356, and 1338 cm^{-1}, indicating a strong electron-molecular vibration (emv) coupling. This band originates from the a_g mode of TTF, which was reported to appear at 1420 cm^{-1} ($a_g\nu_3$) for neutral TTF.[58]

It is emphasized here that the C≡N stretching mode of the fully ionized solids exhibited unexpectedly varied and complicated features depending on the type and size of the counterpart. Figure 3 compares the C≡N stretching modes of neutral CF_3TCNQ molecules with those of some 1:1 fully ionic and segregated solids. The neutral CF_3TCNQ molecule exhibited only one C≡N stretching band at 2223 cm^{-1} (ν_0), which may consist of some C≡N stretching modes. The alkaline and ammonium salts **2**–**6** exhibited several bands at around 2208–2199 (ν_2), 2194–2185 (ν_3), and 2181–2175

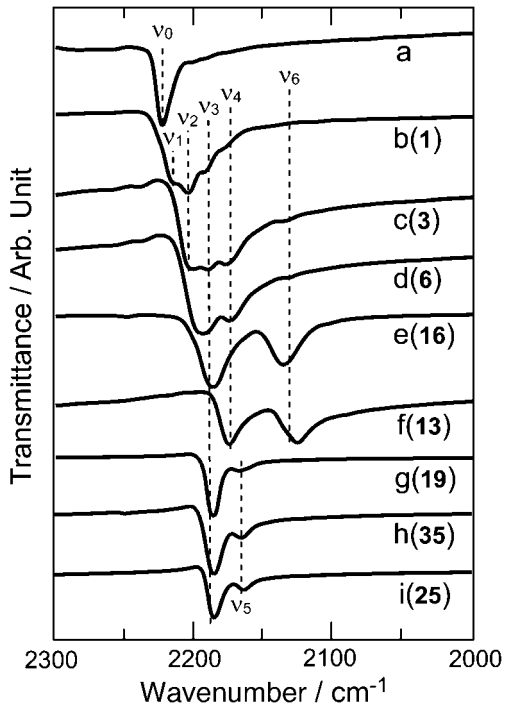

Figure 3. IR spectra in the C≡N stretching region in KBr: a) neutral CF_3TCNQ, and fully ionic 1:1 CF_3TCNQ complexes with b) Li (**1**), c) K (**3**), d) Cs (**6**), e) TMPD (**16**), f) DBPT (**13**), g) $Fe(C_5Me_5)_2$ (**19**), h) TMTTF (**35**), and i) C_1TET-TTF (**25**) complexes. For ν_0–ν_6 bands, see text. Dotted lines are guides.

(ν_4) cm^{-1}. The Li salt **1** exhibited a weak band at 2132 (ν_6) cm^{-1}, in addition to ν_1–ν_4. The ν_6 band appeared weakly for **3**–**7**. Using a very large molecule as a counterpart, the shape of the C≡N stretching bands was appreciably modified; that is, **13**, **16**, and **19** exhibited ν_3, ν_4, ν_5, and/or ν_6 modes. Therefore, the shift of the C≡N stretching modes cannot be used to estimate quantitatively the degree of CT in the CF_3TCNQ complexes, unlike the TCNQ complexes.[63] Instead, the total shape in the C≡N stretching region in spectra b–i in Figure 3 is utilized to identify the fully ionic state of CF_3TCNQ. The origin of the multiple C≡N stretching is discussed below.

Fully Ionic Complex with DDAA Stack (Type IA2) and Triplet Exciton. C_1TET-TTF·CF_3TCNQ (**25**) and TMTTF·CF_3TCNQ·MeCN (**35**) belong to this group and their D:A ratio is 1:1. They exhibited nearly the same C≡N stretching frequencies (Figure 3). The other IR bands ascribable to the acceptor are very similar to those of **1** as seen in Table 4 for **35**, indicating that the acceptor moiety is completely ionized and the average charge on the donor moiety is +1 in these 1:1 complexes. Both complexes form $(D^{\bullet+}D^{\bullet+})(A^{\bullet-}A^{\bullet-})$ alternating stacks (vide infra). The packing essentially originates from both the low symmetry and strong electron accepting ability of the CF_3TCNQ molecule, since the radical anions are able to cancel both the net dipole moments and degree of spin freedom by forming a dimer with an inversion center at the midpoint of the dimer. Therefore, the crystal packing is entropy driven. Type **IA2** solids are featured by the characteristic IR and UV–vis–NIR spectra and triplet excitons (vide infra). Other CT solids most probably classified in this group are **14** and **36**–**38**.

Crystal Structures of 25 and 35: The crystallographic data of solids **25** and **35** are summarized in Table 5. The geometry, interatomic distances, and bond angles of the CF_3TCNQ molecules are shown in Table 6. The molecular and crystal structures of **35** and **25** are shown in Figures 4 and 5, respectively.

On the ionization, bond lengths a1–a2, b1–b4, and c1–c2 of CF_3TCNQ (see the figures in Table 6) in **35** and **25** showed a reasonable change from quinoid to benzenoid skeleton. In the case of **35**, the molecular length at the side of the CF_3 group (d2) elongated from 8.77–8.86 to 8.98 Å on ionization, while the molecular width e1 shortened slightly. The bond angles $\alpha 2$ and $\gamma 1$ showed a slight change from those of the neutral molecules. For **25**, the molecular widths e1 and e2 elongated, and differences in bond angles $\alpha 1$, $\gamma 1$, $\delta 1$, and $\delta 2$ were observed upon complexation. Therefore, very diverse conformational change of $CF_3TCNQ^{\bullet-}$, especially around the dicyanomethylene groups, is expected by changing the size and shape of the donor even among the fully ionized CT solids, and that will be the origin of the multiple appearance of the C≡N stretching modes for the $CF_3TCNQ^{\bullet-}$ species. The bond lengths and angles of the TMTTF molecules in **35** are in good agreement with those of the cation state of TMTTF.[64] Although no data have been reported concerning the monocationic state of C_1TET-TTF, the molecular conformation in **25** is similar to that of the partially ionized states ($\delta = 0.5$–0.25) rather than the considerably deformed neutral state.[65] The carbon atom of the CF_3 group is located out of the plane of the TCNQ moiety by 0.25–0.46 Å in the neutral CF_3TCNQ,[13] while it is located on the plane of the TCNQ moiety on complex formation. Two fluorine atoms close to the dicyanomethylene group are located above and below the plane of the TCNQ moiety to diminish the steric hindrance between the CF_3 and dicyanomethylene groups.

The donor and acceptor molecules stack in an alternating manner of DDAA along the $(c + a - b)$ direction for **35** (Figure 4a) and $(c - a)$ direction for **25** (Figure 5a), resulting in poor conductivity. The inversion centers are located at the midpoint of a donor dimer as well as the midpoint of an acceptor dimer.

Figures 4b and 5b show the molecular packing of **35** and **25**, respectively, viewed perpendicular to the molecular plane. Even though both solids have a similar Type **IA2** arrangement along the stacking direction, they have quite different arrangement perpendicular to the stacking direction.

The overlap patterns within a donor dimer and an acceptor dimer, and between donor and acceptor molecules are summarized in Table 7 and in Figure 6, and the schematic views are shown in Figure 7. The CF_3TCNQ dimer exhibited an almost eclipsed overlap of the TCNQ moiety, and the TMTTF dimer also showed an eclipsed overlap. On the other hand, the C_1TET-TTF dimer showed a head-to-tail overlap. The quinoid ring of CF_3TCNQ is nearly on one of the fulvalene rings of TMTTF in **35**, while it is nearly on the central C=C bond of C_1TET-TTF in **25**. In both complexes, the overlap integrals within DD and AA are much larger than those between D and A along the stacking axis. It is noticeable that the overlap integral within a donor dimer is more than twice that within an acceptor dimer. The overlap integrals between the columns are very small.

Table 5. Crystallographic Data of TMTTF·CF_3TCNQ·MeCN (**35**) and C_1TET-TTF·CF_3TCNQ (**25**)

	TMTTF·CF_3TCNQ·MeCN (**35**)	C_1TET-TTF·CF_3TCNQ (**25**)
Formula	$C_{25}H_{18}N_5F_3S_4$	$C_{23}H_{13}N_4F_3S_8$
Formula weight	573.69	658.88
Crystal dimension/mm^3	0.90 × 0.60 × 0.40	0.40 × 0.20 × 0.20
Crystal system	triclinic	triclinic
Space group	$P\bar{1}$	$P\bar{1}$
a/Å	13.1654(7)	11.321(5)
b/Å	13.1498(7)	12.837(5)
c/Å	8.9105(5)	9.864(4)
α/deg	77.604(1)	79.725(5)
β/deg	88.716(1)	82.509(6)
γ/deg	61.067(1)	71.445(5)
V/Å^3	1312.6(1)	1333.0(10)
Z	2	2
D_{calcd}/g cm^{-3}	1.452	1.642
Radiation	Mo Kα	Mo Kα
μ(Mo Kα)/cm^{-1}	4.08	7.14
T/K	300	300
Independent obsd reflections	5951	6089
Reflections with $I > 2\sigma(I)$	4929	4846
Refined parameters	339	364
$wR2$ (for all data)	0.1109	0.1132
R_{gt} (for $I > 2\sigma(I)$)	0.0370	0.0364
GOF	1.026	1.070

Table 6. Interatomic Distances (Å) and Angles (°) of CF_3TCNQ Molecules in Neutral CF_3TCNQ,[13] TMTTF·CF_3TCNQ·MeCN (**35**), and C_1TET-TTF·CF_3TCNQ (**25**)

Distance[a]	Neutral CF_3TCNQ[b]		**35**	**25**	Angle[a]	Neutral CF_3TCNQ[b]		**35**	**25**
	(I)	(II)				(I)	(II)		
a1	1.341(6)	1.344(8)	1.359(2)	1.362(3)	α1	116.7(4)	117.2(5)	117.1(2)	116.0(2)
a2	1.345(7)	1.348(8)	1.372(2)	1.368(3)	α2	122.8(4)	122.4(5)	121.7(1)	122.4(2)
b1	1.454(7)	1.449(8)	1.425(2)	1.428(3)	β1	117.5(5)	116.4(5)	117.0(2)	117.4(2)
b2	1.461(7)	1.456(8)	1.434(2)	1.422(3)	β2	127.3(5)	127.6(5)	127.9(2)	127.6(2)
b3	1.431(7)	1.426(8)	1.407(2)	1.404(3)	γ1	120.2(5)	120.3(5)	119.2(2)	118.9(2)
b4	1.448(7)	1.445(8)	1.413(2)	1.415(3)	γ2	128.2(5)	128.9(5)	129.6(2)	128.6(2)
c1	1.363(8)	1.390(8)	1.419(2)	1.422(3)	δ1	111.6(5)	110.9(5)	110.9(1)	112.5(2)
c2	1.366(7)	1.383(8)	1.424(2)	1.416(3)	δ2	116.8(5)	116.0(5)	116.9(2)	117.8(2)
d1	8.168(7)	8.006(7)	8.078	8.064					
d2	8.771(7)	8.862(7)	8.982	8.820					
e1	4.165(7)	4.149(7)	4.124	4.214					
e2	4.339(7)	4.379(7)	4.364	4.420					

a) Each distance and angle are shown in the figures below. b) Neutral CF_3TCNQ has two crystallographically independent molecules (I, II).

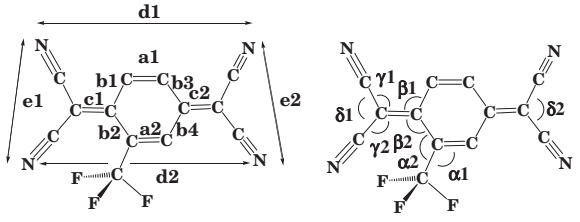

The face-to-face dimerization of the same species, which arises from the asymmetry of the CF_3TCNQ molecule, is the most significant aspect in the complexes. The DDAA stacking is not common, but not so rare as reported for the radical salts of 1,5-dimethylbenzimidazolium·TCNQ,[56a] 1,3,5-trimethylbenzimidazolium·TCNQ,[56b] NBP·F_4TCNQ,[56c] NBP·TCNQ,[56d] 3,3′-diethyloxacyanine·TCNQ,[56e] and 1-ethyl-2,3-dimethylimidazolium·TCNQ,[56f] and for the DA type CT solids of phenothiazine·bis(trifluoromethylethylene-1,2-dithiolato)-nickel),[56g] (TTF)(thiophene-fused TCNQ),[56n] dimethyl-TTF·

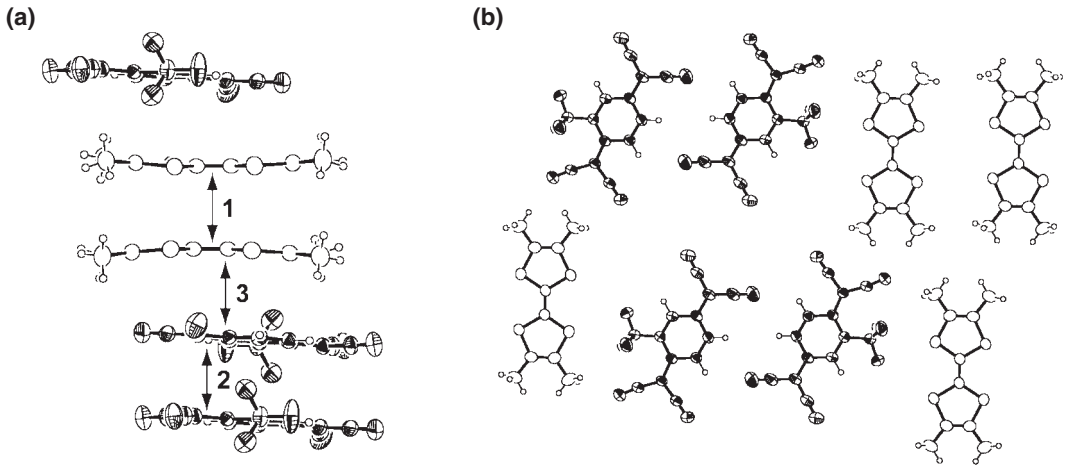

Figure 4. Molecular and crystal structures of **35**. (a) Side view of a donor–acceptor column. (b) Crystal structure viewed perpendicular to the molecular plane. In both figures, acetonitrile molecule is omitted to simplify, and the atoms of CF_3TCNQ are shaded. In Figure 4a, the numbers correspond to the overlap integrals in Table 7.

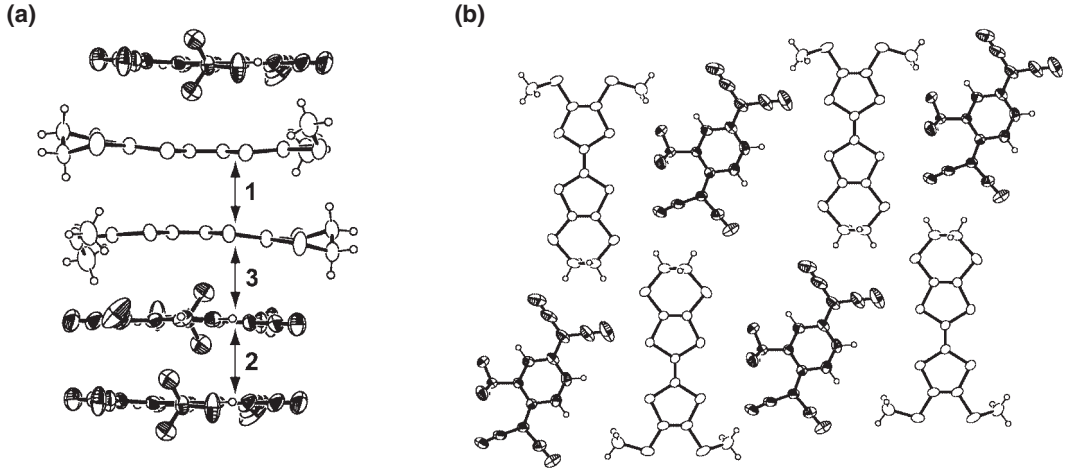

Figure 5. Molecular and crystal structures of **25**. (a) Side view of a donor–acceptor alternating column. (b) Crystal structure viewed perpendicular to the molecular plane. Other comments are the same as those in Figure 4.

TCNE,[56i] [(±)Me_3TTF-CH(Me)OH]·TCNQ,[56j] TTF·TCNE,[56k] (TTF)(DCNQI derivatives),[56l] TTC_1-TTF·TCNQ,[56m] and TSC_1-TTF·TCNQ,[56n,56o] where NBP, TCNE, and DCNQI are 5-(1-butyl)phenazinium, tetracyanoethylene, and dicyanoquinodiimine, respectively. Except for the last two neutral ones, they have a fully ionic ground state (Type **IA2**), and all of them are insulators. The characteristic feature of the complexes in Refs. 56a–56e and 56j is that the asymmetry of the cation or donor species led to the formation of the cation dimer with an inversion center in the middle of the dimer and gave rise to the $(D^{\bullet+}D^{\bullet+})(A^{\bullet-}A^{\bullet-})$ alternating stacks. Triplet excitons have been detected in the complexes in Refs. 56c–56e and 56j.

Optical Properties of 25 and 35: One of the consequences of donor dimerization is the appearance of the IR inactive a_g mode of the donor molecules. For example, the a_g modes appeared at 1545, 1356, 931, and 504 cm^{-1} in the TMTTF complex **35** (Table 4), which have been assigned as $a_g\nu_3$, $a_g\nu_4$, $a_g\nu_8$, and $a_g\nu_{10}$, respectively.[59]

The UV–vis–NIR spectra of the 1:1 complexes of Type **IA2** (**25** and **35**–**38**) have different features from those expected by eq 4 and have a characteristic band in the region of 10–20 $\times 10^3$ cm^{-1}. A typical example is that of **35** (c in Figure 8), where a broad band with peaks at 11.3, 12.8, 14.1, and 17.2 $\times 10^3$ cm^{-1} was observed.

The spectral comparison between $CF_3TCNQ^{\bullet-}$ in Figure 2b and $TMTTF^{\bullet+}$ in Figure 8 (a in solution and b in KBr) allows the assignments of the spectrum of **35**: The band at 11.3 $\times 10^3$ cm^{-1} stems from the transition between the dimerized $CF_3TCNQ^{\bullet-}$ molecules ($A^{\bullet-} + A^{\bullet-} \rightarrow A^{2-} + A^0$; C_2'-band), which located at a higher energy compared to the B′-band in solid K·CF_3TCNQ. The band at 14.1 $\times 10^3$ cm^{-1} is ascribed to the intramolecular transition of $CF_3TCNQ^{\bullet-}$ (D′-band). Similarly, the band at 12.8 $\times 10^3$ cm^{-1} is assigned to the intradimer transition of the dimerized TMTTF cations ($D^{\bullet+} + D^{\bullet+} \rightarrow D^{2+} + D^0$; C_2-band), which shows a substantial blue-shift compared to the B-band in solid TMTTF·Br (ca. 10 $\times 10^3$ cm^{-1}). The CT transition from $A^{\bullet-}$ to $D^{\bullet+}$ (so-called back CT; eq 4), whose absorption band may weaken as the overlap integral between D and A is reduced and is expected to appear at 6.7–8.6 $\times 10^3$ cm^{-1} based on the $h\nu_{CT}$(TMTTF·TNB) value,

Table 7. Interplanar Distances, Dihedral Angles, and Overlap Integrals of TMTTF·CF_3TCNQ·MeCN (**35**) and C_1TET-TTF·CF_3TCNQ (**25**)

	35			25		
	Distance/Å	Angle/°	Overlap integral/10^{-3}	Distance/Å	Angle/°	Overlap integral/10^{-3}
(1) Donor–donor	3.5	0.0	51.5	3.5	0.0	42.6
(2) Acceptor–acceptor	3.4	0.0	−22.0	3.4	0.0	−20.4
(3) Donor–acceptor	3.5	≈6	−3.0	3.5	≈3	0.2

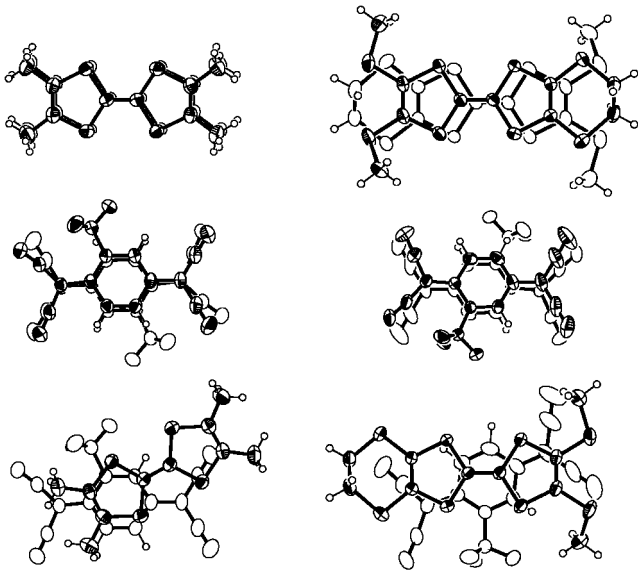

Figure 6. Overlap patterns of donor and acceptor molecules viewed perpendicular to the molecular planes in TMTTF·CF_3TCNQ·MeCN (**35**, left) and in C_1TET-TTF·CF_3TCNQ (**25**, right). The donor–donor (top), acceptor–acceptor (middle), and donor–acceptor (bottom) pairs correspond to those denoted as **1**, **2**, and **3**, respectively, in Figures 4 and 5 and Table 7. The shaded molecules represent the top ones.

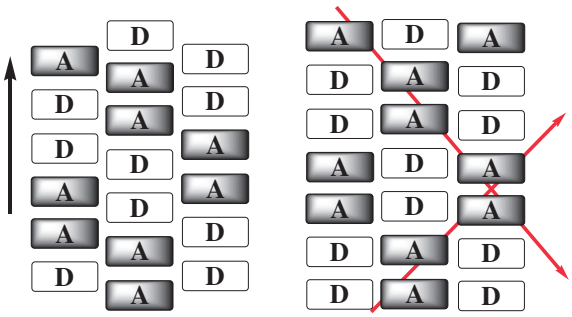

Figure 7. Schematic views of the packing pattern of DDAA in **35** (left) and **25** (right). A vertical arrow indicates the stacking axis. Red arrows in the C_1TET-TTF complex indicate the directions, where two EPR signals merge in Figure 9.

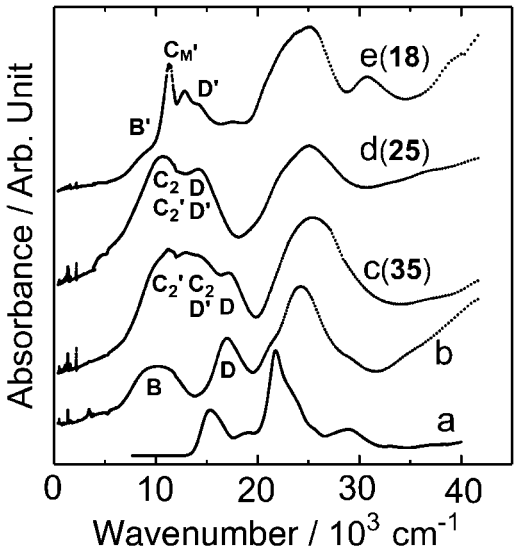

Figure 8. Optical absorption spectra of fully ionic complexes: a) TMTTF·Br in MeOH, b) TMTTF·Br in KBr, c) TMTTF·CF_3TCNQ·MeCN (**35**) in KBr, d) C_1TET-TTF·CF_3TCNQ (**25**) in KBr, and e) (TDAP)$(CF_3TCNQ)_2$·H_2O (**18**) in KBr. For bands B, B′, C_2, C_2′ and C_M′, see text.

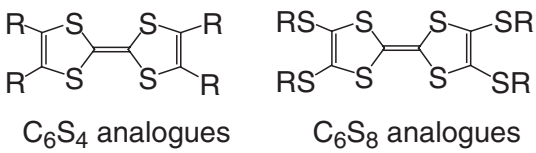

Scheme 2. C_6S_4 and C_6S_8 skeletons.

was not observed in spectrum of **35**. The absence of the back CT band is a similar feature to the case of a BEDT-TTF·F_2TCNQ single crystal (fully ionic alternating stacks with poor donor–acceptor interactions).[54]

Since the donor molecule in **25**, C_1TET-TTF, has an extended π-system (C_6S_8 analogs; Scheme 2), B-, C-, and D-bands appear at a considerably lower energy compared to those of TTF derivatives such as TTF, TMTTF, HMTTF, and OMTTF, which contain no peripheral chalcogen atoms (C_6S_4 analogs).[16k,16l,66] As a result, C_2- and D-bands overlap with C_2′- and D′-bands, respectively, in **25** as represented by spectrum d in Figure 8.

Magnetic Properties: Triplet Exciton: The other consequence of the dimerization of radical molecules is the charge localization and pairwise antiferromagnetic coupling of electron spins to show triplet excitons. Figure 9 shows the angular dependence of the EPR signals of **25** at RT with the external magnetic field H_0 residing in the largest crystal plane.

The crossing point, where two resonances merge, corresponds to the direction inclined from the stacking axis by 50 degrees (Figure 7). The peak-to-peak linewidth ΔH is 2.0–2.1 mT when H_0 is parallel to the molecular plane, while it increases along the stacking direction (2.7 mT), where moving of the triplet exciton is forbidden due to the alternating column

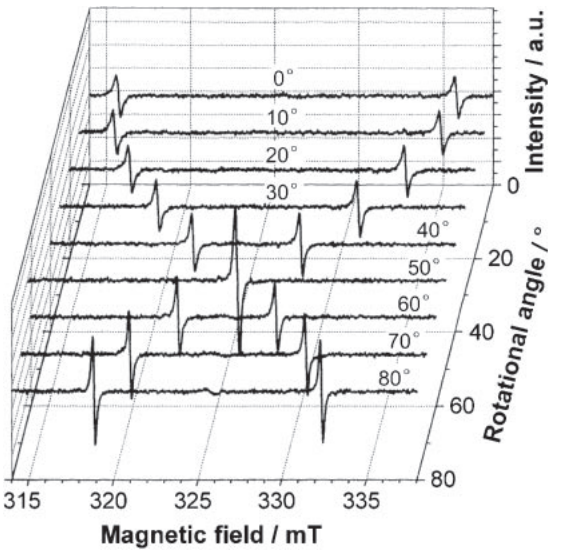

Figure 9. Angular dependence of room temperature EPR spectrum of a single crystal of C_1TET-TTF·CF_3TCNQ (**25**). The external field (H_0) is in the largest crystal plane. Maximal splitting corresponds to H_0//long crystal axis (stacking axis).

of acceptor and donor dimers (Figure 7). The *g*-factor is minimal along the stacking axis ($g = 2.0020$) and increases along the molecular plane ($g = 2.0031$–2.0032), and the values are typical for TCNQ-based salts. The splitting of the signals is 20 mT when H_0//stacking axis and 8–18 mT when H_0//molecular plane. Judging by the orientation of the splitting and the *g*-value, it is concluded that only a Frenkel triplet spin exciton originating from the CF_3TCNQ dimer is observed. No appearance of the triplet signal originating from the donor dimer is associated with a much larger overlap integral within the donor dimer than that within the acceptor dimer (Table 7).

The facts that the signals show no exchange narrowing and no hyperfine splitting indicate that the exciton moves, but its movement is slow, just enough to compensate the hyperfine structure. This is the so-called quasi-immobile Frenkel exciton,[56d] and the spin concentration at RT is $(1.0 \pm 0.5) \times 10^{-3}$ spins per formula unit. Using the triplet spin Hamiltonian (eq 8),

$$H = D(S_z^2 - 2/3) + E(S_x^2 - S_y^2) \quad (8)$$

and the principal values of the splitting, the fine structure constants D and E, and the ratio D/E are determined as −42.0 mT, 5 mT, and −8.4, respectively. These values are comparable to those of NBP·F_4TCNQ (−38.6 mT, 6.8 mT, and −5.7),[56c] NBP·TCNQ (−42.1 mT, 6.4 mT, and −6.6),[56d] and [(±)Me_3TTF-CH(Me)OH]·TCNQ (−40.3 mT, 5.5 mT, and −7.3).[56j]

The triplet signals decreased in intensity with decreasing temperature, and extinguished below 200 K. Triplet excitons are thermally activated following the empirical formula:

$$I(T) = (I_0/T)\exp(-E_a/k_BT) \quad (9)$$

where I is the intensity, and E_a is the activation energy which was estimated to be 0.20–0.28 eV.

1:2 Fully Ionic Complex (Type IS or IA). The TDAP molecule is a strong electron donor[16n,67] and displays a reversible two-electron redox wave at $E^{0/2+} = +0.02$ V vs. SCE in MeCN. This donor molecule afforded a 1:2 solid with CF_3TCNQ, i.e., (TDAP)$(CF_3TCNQ)_2 \cdot H_2O$ (**18**), as green powder. The C≡N stretching modes appeared at 2184 (ν_3) and 2163 (ν_5) cm^{-1}, and the total shape in the C≡N stretching region is very similar to those of the 1:1 fully ionic complexes of strong donor **19** and with DDAA stack (**25** and **35**) (Figure 3). Therefore, the complex is concluded to be composed of TDAP dications and CF_3TCNQ radical anions. The UV–vis–NIR spectrum, which is shown as spectrum e in Figure 8, exhibited a C′-band with a fine structure similar to that observed in K·CF_3TCNQ in solution (c in Figure 2b). These results indicate that **18** includes isolated monomers of $CF_3TCNQ^{\bullet-}$ (C_M′-band). The presence of a shoulder at around 8.5×10^3 cm^{-1} is indicative of either the presence of the segregated column of $CF_3TCNQ^{\bullet-}$ (B′-band) or backed CT from $CF_3TCNQ^{\bullet-}$ to $TDAP^{2+}$ ($h\nu_{CT}^{I}$) within the alternating $D^{2+}A^{\bullet-}A^{\bullet-}$ stack. The CF_3TCNQ molecules in **18** may form rather complicated stacks with both isolated and segregated natures.

Mixed-Valence Solid with Deficient Acceptor Molecules. Solids **15**, **21**–**24**, **26**–**30**, **33**, and **34** belong to this group and exhibit A-bands. All of them consist of excess donors; that is, in addition to the conventional 2:1, 5:3, and 4:3 ratios, some have uncommon compositions of D:A = 6:5 (**15**) and 10:9 (**30**). The CF_3TCNQ molecules in these complexes are fully ionized. Thus, the acceptor deficiency (A/D = 0.5–0.9) results in the formation of conductive DA solids with mixed valence donor species, where acceptor species act as counter anions.

Mixed-Valence Solid with Segregated Stack (Type MS): The UV–vis–NIR spectra of the 2:1 solids (**26**, **28**, **29**, and **34**) and 10:9 TTF complex (**30**) in Figure 10 show the A-band indicating that the segregated stacks of mixed valence donor molecules exist. The band weakly appearing 7–9 $\times 10^3$ cm^{-1} is assignable mainly to the B′-band since the B-band should not have appreciable intensity for 2:1 solids.[55] The broad B′-band in the TTF complex **30** may overlap with the B-band. The C′-band was clearly seen as a peak at 11.5–11.6 $\times 10^3$ cm^{-1} in **26**, **28**, and **34**, indicating a lattice distortion in the CF_3TCNQ column (C_D′-band). In **29**, the C′-band is rather broad due to the overlap with C- and/or D-bands.

Figure 11 compares the UV–vis–NIR spectra of BEDT-TTF complexes (5:3:1PhCl (**21**), 5:3 (**23**), and 2:1 (**24**)), 4:3 HMTTeF complex **27**, and 2:1 TMTSF complex **33**. For the BEDT-TTF complexes, the sharp and narrow peak observed at around 11 $\times 10^3$ cm^{-1} (C′-band) as seen in Figure 10 cannot be identified. The broad band at 10–12 $\times 10^3$ cm^{-1} appearing for the BEDT-TTF complexes is ascribed to the intramolecular transition (D-band: second HOMO → HOMO).[16k,16l,66] Therefore, the narrow C′- and broad D-bands overlap with each other to give a broad band at around 11 $\times 10^3$ cm^{-1}, resulting in the different spectral feature from those of the other CF_3TCNQ complexes. Among the four BEDT-TTF complexes obtained in this work, the significant difference in the spectra is seen by the appearance of a very weak B′-band at ca. 7–8 $\times 10^3$ cm^{-1} in **24**.

The sharp appearance of a fine structure in the C′-band along with the lack of the B′-band in the HMTTeF complex **27**

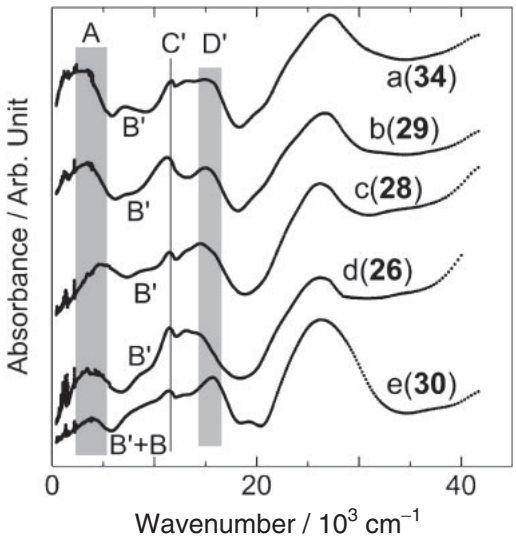

Figure 10. Optical absorption spectra of mixed valence 2:1 CF_3TCNQ complexes with a) BEDO-TTF (**34**), b) EOET (**29**), c) EDT-TTF (**28**), and d) BEDO-DBTTF (**26**), in addition to e) $(TTF)_{10}(CF_3TCNQ)_9 \cdot 3THF$ (**30**). For bands A, B′, C′, and D′, see text. Vertical lines are guides.

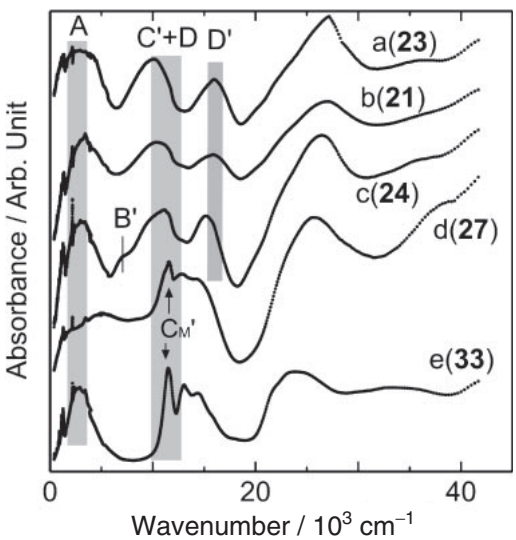

Figure 11. Optical absorption spectra of mixed valence complexes: a) 5:3 (**23**), b) 5:3:1PhCl (**21**), and c) 2:1 (**24**) BEDT-TTF complexes, d) 4:3 HMTTeF complex (**27**), and e) 2:1 TMTSF complex (**33**). For bands A, B′, C′, C_M′, D′, and D, see text. Vertical lines are guides.

indicates the isolated nature of the anion molecules (C_M′-band). The weak absorption at around 5–8 $\times$ 10^3 cm^{-1} is ascribed to the B-band. A similar isolated nature of anion molecules is observed in the 2:1 TMTSF complex **33**.

Figure 12 compares the vibrational spectra of **24**, **29**, and **34** together with those of **33** and **1** in the region of 1600–400 cm^{-1}, and the assignments of the main signals are summarized in Table 4. It is noteworthy that an electronic transition overlaps considerably with the vibrational signals in the highly conductive complexes (spectra a–d), in contrast to the sharp signals observed in the insulating complex **1** (spectrum e). The

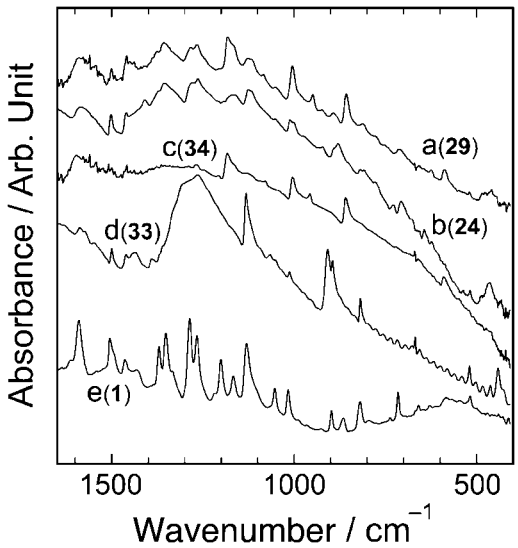

Figure 12. IR spectra in the region of 1600–400 cm^{-1} of the highly conductive 2:1 CF_3TCNQ complexes with a) EOET (**29**), b) BEDT-TTF (**24**), c) BEDO-TTF (**34**), and d) TMTSF (**33**) are compared with that of e) $Li \cdot CF_3TCNQ \cdot 0.75H_2O$ (**1**).

main IR signals of **24**, **29**, and **34** are essentially derived from those of the donor molecules, where the signals observed in the EOET complex **29** are the superimposition of those of BEDT-TTF (**24**) and BEDO-TTF (**34**) complexes in good agreement with the hybridized molecular structure of EOET. Characteristic bands of $CF_3TCNQ^{\bullet -}$ molecules appeared at around 1500 and 1130 cm^{-1}. The appearance of the strong emv coupling and a_g mode in **33** and **34** suggests the non-uniform lattice as summarized in Table 3.

Metallic Conductivity on Pellet Samples and LB Films: The appearance of the strong A-band in **29** and **34** (spectra a and b in Figure 10) implies good conductivity. In fact, they are metallic even in the compressed pellet samples (Figure 13), suggesting the enhanced dimensionality. The pellet sample of **34** ($\sigma_{RT} = 1.7 \times 10^2$ S cm^{-1}) was metallic down to 1.8 K despite the distortion in donor lattice, while that of **29** ($\sigma_{RT} = 5.8$ S cm^{-1}) showed a metal–insulator transition at around 250 K. Since the self-assembling ability of BEDT-TTF is inferior to EOET and BEDO-TTF, BEDT-TTF salts exhibited semiconductive behavior, at least, on the compressed pellets. **24** showed a finite activation energy ($\sigma_{RT} = 4.2$ S cm^{-1}, $\varepsilon_a = 32$ meV).

The σ_{RT} value of the compressed pellet of **34** is higher than those of BEDO-TTF complexes with MeTCNQ (2:1, 5.0 $\times$ 10 S cm^{-1}), $(MeO)_2TCNQ$ (2:1, 4.7 $\times$ 10 S cm^{-1}), $C_{10}TCNQ$ (10:4:H_2O, 7.3 S cm^{-1}), and $C_{14}TCNQ$ (9:4:2H_2O, 0.99 S cm^{-1}).[16k] The former three solids are metallic down to low temperatures (ca. 1.4 K), while the $C_{10}TCNQ$ complex is metallic down to 136 K and the $C_{14}TCNQ$ complex is semiconducting. The electrical conductivity of these BEDO-TTF complexes is attributable to the mobile holes on the BEDO-TTF molecules, while the acceptor molecules act as counter anions even though their ΔE(DA) values are in the mixed valence region. It is obvious that the bulkiness of the substituent groups on TCNQ moiety provides retarding events for electrical transport in the pellet samples.

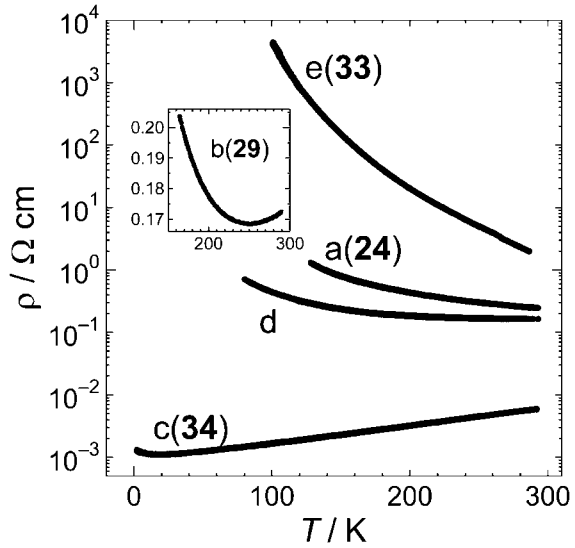

Figure 13. Temperature dependence of resistivity of a) $(BEDT\text{-}TTF)_2(CF_3TCNQ)$ (**24**), b) $(EOET)_2(CF_3TCNQ)$ (**29**) (inset), and c) $(BEDO\text{-}TTF)_2(CF_3TCNQ)$ (**34**) on compressed pellets, d) $(BEDO\text{-}TTF)_2(CF_3TCNQ)$ on LB film, and e) $(TMTSF)_2(CF_3TCNQ)$ (**33**) on a single crystal.

As reported in our brief paper,[68] the 10-layer mixed LB films of **34** and arachidic acid in a mixing ratio of 2:1 are highly conductive ($\sigma_{RT} = 3$–$6\,S\,cm^{-1}$ assuming the thickness of each monolayer as 2.3 nm). The conductivity of the film was independent of temperature near RT, and neither obvious metallic dependence nor drastic change into an insulating state were detected down to 80 K (d in Figure 13).

The σ_{RT} values of LB films based on BEDO-TTF are 11.3, 10.4, and $3.0\,S\,cm^{-1}$ for the $(MeO)_2TCNQ$, $C_{10}TCNQ$, and $C_{14}TCNQ$ complexes, respectively.[4] It is noteworthy that the σ_{RT} values of the LB films composed of the complexes of TCNQs with a long alkyl chain are superior to those of the corresponding compressed pellet samples. Because the molecular orientation in the LB films is thought to be more ordered than that in the compressed pellet sample, it is reasonable to have higher σ_{RT} values in the LB films than in the pellet samples of the $C_{10}TCNQ$ and $C_{14}TCNQ$ complexes. However, much lower σ_{RT} values and poorer metallic temperature dependence observed in the LB films than those in the pellet samples of the CF_3TCNQ and $(MeO)_2TCNQ$ complexes are ascribed to the imperfectly ordered structure in the LB films due to the poor hydrophobicity of TCNQs with short substituent group(s).

TMTSF Complex 33 (Type MS). Two kinds of TMTSF complexes (1:1:1/2PhCl fine needles (**32**) and 2:1 plates (**33**)) were harvested simultaneously from PhCl and were separated under a microscope according to their shapes. **32** belongs to Type **IS** as described. Another TMTSF complex **33** exhibited a very sharp A-band at $2.6 \times 10^3\,cm^{-1}$ (Figure 11), which confirms the presence of the segregated stacks. The sharp C′-band with a fine structure at 11.5 and $13.1 \times 10^3\,cm^{-1}$ indicates the isolated nature of the $CF_3TCNQ^{\bullet-}$ molecules (C_M′-band), in good agreement with the structural analysis (vide infra). The IR spectrum of **33** (Figure 12 and Table 4) showed a broad strong band between 1100 and $1400\,cm^{-1}$ with a peak around

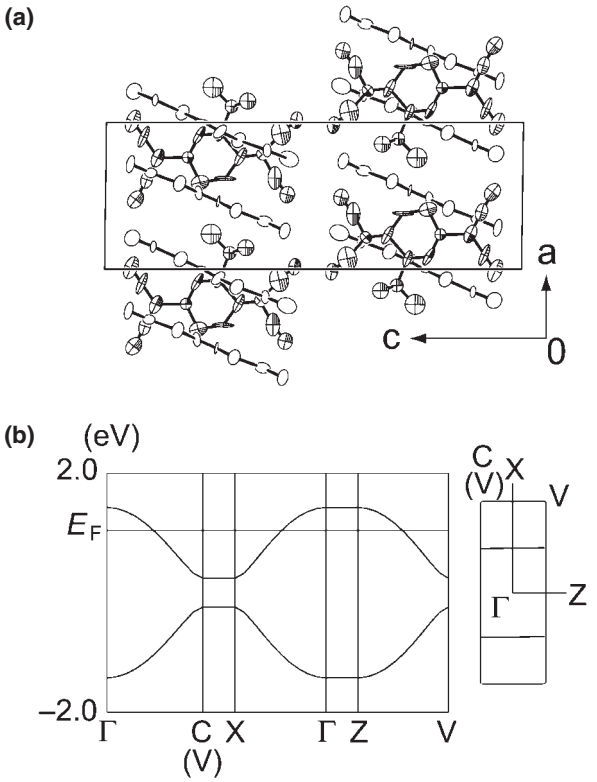

Figure 14. (a) Crystal structure of $(TMTSF)_2(CF_3TCNQ)$ (**33**) viewed along the *b* axis showing TMTSF segregated columns sandwiched by CF_3TCNQ molecules. The molecular plane of CF_3TCNQ is perpendicular to that of the TMTSF molecules. (b) Energy dispersion and Fermi surface of **33** calculated by extended Hückel method with tight binding approximation including Se 3d orbitals based on the crystal structure.

$1290\,cm^{-1}$ ($a_g\nu_4$), indicating a strong emv coupling together with lattice distortion.

Due to the poor quality of crystal **33**, the crystal structure analysis gave a rather large *R*-value (0.141) and the molecular structure is not discussed in detail. The crystallographic data, molecular structures of the crystallographically independent two TMTSF and one CF_3TCNQ molecules, and the overlapping pattern of the TMTSF dimers are presented in the Supporting Information (Tables S2 and S3). The molecular packing viewed along the *b* axis is depicted in Figure 14a.

Along the *a* axis, dimerized TMTSF molecules form a segregated column, which is sandwiched by columns of CF_3TCNQ molecules. A preliminary band structure calculated by the extended Hückel method with tight binding approximation using single-ζ parameters including Se 3d but excluding Se 4f orbitals suggests the presence of a complete one-dimensional Fermi surface (Figure 14b). The molecular plane of $CF_3TCNQ^{\bullet-}$ is parallel to the stacking direction of the TMTSF column. Therefore, the $CF_3TCNQ^{\bullet-}$ acts as a counter anion and locates between the donor segregated columns with their molecular planes almost perpendicular to the donor molecular plane, as has been observed for squarate and other anions in metallic BEDO-TTF complexes,[16k] aza-TCNQ in $(TMTTF)_2$(aza-TCNQ) and $(TMTSF)_2$(aza-TCNQ),[32a] hexa-

cyanobutadiene (HCBD) in $(TMTTF)_2(HCBD)$,[32b] cyananilate (HCNAL) in $(BEDT\text{-}TTF)_2(HCNAL)$,[33a] tetranitrobiphenyldiolate (TNBP) in $(TMTTF \text{ or } TMTSF)_2(TNBP)$,[33b] and Cl_2TCNQ in $(BEDT\text{-}TSF)_2(Cl_2TCNQ)$.[2] The isolated nature of $CF_3TCNQ^{\bullet-}$ for **33** is in excellent agreement with the observation of a sharp C_M'-band in Figure 11. The X-ray diffraction measurement suggests the presence of a superstructure of $2a \times b \times c$ at RT. Therefore, the semiconductive nature ($\sigma_{RT} = 0.5\,S\,cm^{-1}$ and $\varepsilon_a = 100$ meV on the single crystal, Figure 13) is most likely associated with Peierls distortion in TMTSF column due to both the strong electron–phonon interactions and the extreme one-dimensional electronic nature (Type **MuSn**).

Ionicity Diagram for CF_3TCNQ CT Solids

In this work, the CT solids of **IA2** (**14**, **25**, and **35–38**), **IS** (**1–7**, **13**, **16–19**, **31**, and **32**), **MS** (**15**, **21–24**, **26–30**, **33**, and **34**; they cannot be discriminated between **MuSu** and **MuSn**, except metallic **MuSn 34** and highly conductive **MuSn 33**), and **NA** (**8–12** and **20**) have been obtained. In the following, we describe the ionicity phase diagram of the CF_3TCNQ CT solids, which include the regions for **IS** and **IA2** that were not allocated in Figure 1b. Since the redox potentials of some donor molecules and cations in Tables 1–3 are not available, we used the $h\nu_{CT}(D\cdot TNB)$ values in the diagram (Figure 15) as a measure of donor strength.

The diagram shows a plot of the first CT absorption band of CT solids in KBr against $h\nu_{CT}(D\cdot TNB)$. Four groups are clearly discriminated, i.e., Group **i**: insulating neutral solids residing near the right branch of the V-shaped line (**NA**), Group **ii**: highly conductive solids with mixed valence segregated stacks, donor excess, fully ionized acceptor, and showing the A-band (**MS-1**), Group **iii**: insulating 1:1 solids having fully ionic ground states with segregated stacks and showing the B′-band at $8.5–10.5 \times 10^3\,cm^{-1}$ (**IS**), and Group **iv**: insulating 1:1 solids having fully ionic ground states with $D^{\bullet+}D^{\bullet+}A^{\bullet-}A^{\bullet-}$ stacks and showing the C_2- or C'_2-band at $10.8–11.6 \times 10^3\,cm^{-1}$ (**IA2**). According to the classification in Figure 15, the following remarks are made.

1) A rough boundary of ionization, which is drawn by a thick gray vertical line in Figure 15, is observed at $h\nu_{CT}(D\cdot TNB) = 17.1–17.3 \times 10^3\,cm^{-1}$ (**13**, **14**, and **20**).

2) In the CT solids with stronger donors than DBTTF (donor in **20**), CF_3TCNQ molecules have a strong tendency to be fully ionized rather than to be partially ionized, even though all their DA redox differences are within the two boundaries in Figure 1a. Thus, no partial CT state of CF_3TCNQ with 1:1 stoichiometry and segregated stacks has so far been identified in the DA CT solids. This is a remarkable difference from the case of the pristine TCNQ,[1,28] which has afforded a variety of CT solids of **MS** group. However, the observed situation in this work is similar to the fact that the TCNQ derivatives in the complexes with BEDO-TTF (D:A = 2:1, R-TCNQ: R = Me, $(MeO)_2$, C_{10}, and C_{14}),[16k] BEDT-TSF (D:A = 2:1, R = Cl_2),[2] and BEDT-TTF (D:A = 1:1, R = F_2)[55] are fully ionized.

3) In the CT solids with strong donors, the CF_3TCNQ molecules act as counter anions and afford highly conductive solids in Group **ii** when the donor molecule is slightly (A/D = 0.8–0.9, **15** and **30**) or considerably (4:3, 5:3, and 2:1 solids; A/D = 0.5–0.75, **21–24**, **26–29**, **33**, and **34**) excess in ratio. In the latter case, the donor molecules are TTF derivatives having self-aggregating ability. A typical example is $(BEDO\text{-}TTF)_2(CF_3TCNQ)\cdot 0.5H_2O$ (**34**), which shows metallic behavior in the compressed pellet sample and a nearly temperature-independent conductivity in the LB film. On the other hand, donor molecules having a weak self-assembling ability such as pristine TTF and $Fe(Cp)_2$ afforded conductive solids **15** and **30** with considerably high donor ionicity $\delta = 0.8–0.9$. The range of donor strength in Group **ii** is very narrow as scaled by the $h\nu_{CT}(D\cdot TNB)$ values of $14.9–16.1 \times 10^3\,cm^{-1}$. The range of $1.2 \times 10^3\,cm^{-1}$ corresponds to $\Delta E(DA) = 0.15$ V, which is much narrower than those for TTF·TCNQ family (0.37 V)[16b] and BEDO-TTF complexes (0.85 V).[16k]

4) Strong donors having a weak self-assembling ability, such as aromatic amines, azines, alkali metals, oniums and several TTF derivatives (TTF, TMTTF, HMTTF, OMTTF, and C_1TET-TTF; the terminal thiomethyl groups of C_1TET-TTF suppress the self-assembling ability though it belongs to the C_6S_8 analogs) afforded the solids in Groups **iii** and **iv** when the composition is 1:1. The observation of the B-band indicates that the solids in Group **iii** have segregated stacks instead of the $D^{\bullet+}A^{\bullet-}$ alternating stacks. In addition, the low symmetric $CF_3TCNQ^{\bullet-}$ molecule preferably forms entropy driven $A^{\bullet-}A^{\bullet-}$ dimers to give rise to the CT solids in Group **iv** with a $D^{\bullet+}D^{\bullet+}A^{\bullet-}A^{\bullet-}$ stack, which is able to generate triplet exciton.

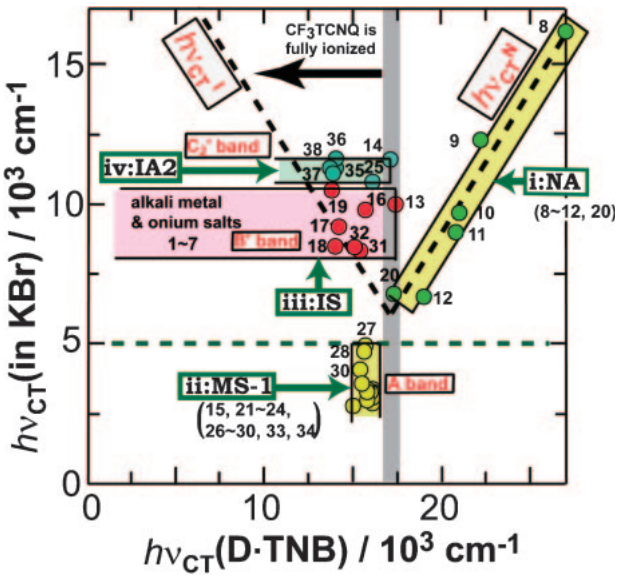

Figure 15. Classification of CF_3TCNQ CT solids by a plot of $h\nu_{CT}$ in KBr against $h\nu_{CT}(D\cdot TNB)$. Group **i**: neutral insulators (green circles), Group **ii**: conductors having partial CT and segregated columns (yellow circles), Group **iii**: insulators having fully ionic segregated columns (red circles), and Group **iv**: insulators having fully ionic DDAA stacks (blue circles). V-shaped line represents eqs 2 and 3 and is a guide to separate the neutral (right) and ionic (left) CT solids. The horizontal line at $h\nu_{CT}(\text{in KBr}) = 5 \times 10^3\,cm^{-1}$ is to discriminate the conductive (below the line) and less-conductive (above the line) CT solids. Thick vertical gray line indicates the boundary for ionization. For each group, the origin of the lowest energy optical absorption band is indicated.

5) The solids **17**–**19**, **31**, and **32** in Group **iii** are allocated not far from the line of $h\nu_{CT}^{I}$, which makes it difficult to classify them into either Type **IA** or **IS**. Though structural analysis is the best way to know the stacking mode, a detailed comparison of the solid-state UV–vis optical data in the range of 5–$40 \times 10^3\,cm^{-1}$ between the CT complexes and the ion radical salts of the component molecules provides sufficient information about the stacking manner of these types of solids.

6) Ionicity phase diagram Figure 15 is convenient to search for a possible candidate for a) N–I system which is expected to reside near the bottom of the V-shaped line in the neutral side, b) 1:1 Mott insulator which is expected to belong to Group **iii** and show no lattice distortion, c) narrow gap semiconductor based on charge-ordered system, spin-Peierls system, dimer-type Mott insulators with $\delta = 0.5$ and $U_{eff} > W$, or misfit system, which is expected to exhibit band-A near 5×10^3 cm^{-1}, and d) alternate solid with $D^{\bullet+}D^{\bullet+}A^{\bullet-}A^{\bullet-}$ which may exhibit triplet excitons arising from the $D^{\bullet+}D^{\bullet+}$ and/or $A^{\bullet-}A^{\bullet-}$ pairs depending on both the pairing strength and transfer interactions between the pairs, based on only CT energies.

We are very grateful to Professor Yoshio Matsunaga for useful discussions and comments.

Supporting Information

Elemental analysis of the solids in Tables 1–3 (Table S1) and crystallographic data of $(TMTSF)_2(CF_3TCNQ)$ (**33**) (Tables S2 and S3). This material is available free of charge on the web at http://www.csj.jp/journals/bcsj/.

References

1 J. Ferraris, D. O. Cowan, V. Walatka, J. H. Perlstein, *J. Am. Chem. Soc.* **1973**, *95*, 948.

2 R. Kondo, T. Hasegawa, S. Kagoshima, T. Mochida, Y. Iwasa, *Chem. Lett.* **1999**, 333.

3 Y. Takahashi, T. Hasegawa, Y. Abe, Y. Tokura, G. Saito, *Appl. Phys. Lett.* **2006**, *88*, 073504.

4 a) T. Nakamura, G. Yunome, R. Azumi, M. Tanaka, H. Tachibana, M. Matsumoto, S. Horiuchi, H. Yamochi, G. Saito, *J. Phys. Chem.* **1994**, *98*, 1882. b) K. Ogasawara, T. Ishiguro, S. Horiuchi, H. Yamochi, G. Saito, *Jpn. J. Appl. Phys.* **1996**, *35*, L571.

5 a) Y. Iwasa, N. Watanabe, T. Koda, G. Saito, *Phys. Rev. B* **1993**, *47*, 2920. b) S. Horiuchi, R. Kumai, Y. Okimoto, Y. Tokura, *Chem. Phys.* **2006**, *325*, 78. c) S. Horiuchi, R. Kumai, Y. Okimoto, Y. Tokura, *J. Am. Chem. Soc.* **1999**, *121*, 6757. d) S. Horiuchi, R. Kumai, Y. Tokura, *Chem. Commun.* **2007**, 2321.

6 S. Niwa, *Synth. Met.* **1987**, *18*, 665.

7 a) R. S. Potember, T. O. Poehler, D. O. Cowan, A. N. Bloch, in *The Physics and Chemistry of Low Dimensional Solids*, ed. by L. Alcacer, D. Reidel, Pub. Co., **1980**, p. 419. b) Y. Iwasa, T. Koda, Y. Tokura, S. Koshihara, N. Iwasawa, G. Saito, *Appl. Phys. Lett.* **1989**, *55*, 2111. c) Y. Iwasa, T. Koda, S. Koshihara, Y. Tokura, N. Iwasawa, G. Saito, *Phys. Rev. B* **1989**, *39*, 10441.

8 a) R. M. Metzger, C. A. Panetta, in *Lower-Dimensional Systems and Molecular Electronics*, ed. by R. M. Metzger, P. Day, G. C. Papavassiliou, Plenum, New York, **1990**, p. 611. b) R. M. Metzger, B. Chen, U. Höpfner, M. V. Lakshmikantham, D. Vuillaume, T. Kawai, X. Wu, H. Tachibana, T. V. Hughes, H. Sakurai, J. W. Baldwin, C. Hosch, M. P. Cava, L. Brehmer, G. J. Ashwell, *J. Am. Chem. Soc.* **1997**, *119*, 10455.

9 T. Gotoh, T. Kondoh, K. Egawa, K. Kubodera, *J. Opt. Soc. Am. B* **1989**, *6*, 703.

10 a) G. J. Ashwell, E. J. C. Dawnay, A. P. Kuczynski, M. Szablewski, I. M. Sandy, M. R. Bryce, A. M. Grainger, M. Hasan, *J. Chem. Soc., Faraday Trans.* **1990**, *86*, 1117. b) M. Szablewski, P. R. Thomas, A. Thornton, D. Bloor, G. H. Cross, J. M. Cole, J. A. K. Howard, M. Malagoli, F. Meyers, J.-L. Brédas, W. Wenseleers, E. Goovaerts, *J. Am. Chem. Soc.* **1997**, *119*, 3144.

11 a) H. Endres, in *Extended Linear Chain Compounds*, ed. by J. S. Miller, Plenum, New York, **1983**, Vol. 3, p. 263. b) H. Terauchi, *Phys. Rev. B* **1978**, *17*, 2446.

12 T. Ishiguro, K. Yamaji, G. Saito, *Organic Superconductors*, 2nd ed., Springer-Verlag, Berlin, **1998**.

13 H. Ikegami, C.-H. Chong, H. Yamochi, G. Saito, *Mol. Cryst. Liq. Cryst.* **2002**, *382*, 21.

14 G. M. Sheldrick, *SHELXS-97, Program for the Solution of Crystal Structures*, University of Göttingen, Germany, **1997**.

15 G. M. Sheldrick, *SHELXL-97, Program for the Refinement of Crystal Structures*, University of Göttingen, Germany, **1997**.

16 a) Y. Matsunaga, G. Saito, *Bull. Chem. Soc. Jpn.* **1971**, *44*, 958. b) G. Saito, J. P. Ferraris, *Bull. Chem. Soc. Jpn.* **1980**, *53*, 2141. c) N. Ueda, B. Natsume, K. Yanagiuchi, Y. Sakata, T. Enoki, G. Saito, H. Inokuchi, S. Misumi, *Bull. Chem. Soc. Jpn.* **1983**, *56*, 775. d) G. Saito, T. Enoki, H. Inokuchi, H. Kumagai, J. Tanaka, *Chem. Lett.* **1983**, 503. e) G. Saito, H. Kumagai, J. Tanaka, T. Enoki, H. Inokuchi, *Mol. Cryst. Liq. Cryst.* **1985**, *120*, 337. f) G. Saito, H. Hayashi, T. Enoki, H. Inokuchi, *Mol. Cryst. Liq. Cryst.* **1985**, *120*, 341. g) K. Imaeda, T. Enoki, H. Inokuchi, G. Saito, *Mol. Cryst. Liq. Cryst.* **1986**, *141*, 131. h) G. Saito, T. Teramoto, A. Otsuka, Y. Sugita, T. Ban, M. Kusunoki, K. Sakaguchi, *Synth. Met.* **1994**, *64*, 359. i) T. Akutagawa, G. Saito, *Bull. Chem. Soc. Jpn.* **1995**, *68*, 1753. j) T. Akutagawa, G. Saito, M. Kusunoki, K. Sakaguchi, *Bull. Chem. Soc. Jpn.* **1996**, *69*, 2487. k) S. Horiuchi, H. Yamochi, G. Saito, K. Sakaguchi, M. Kusunoki, *J. Am. Chem. Soc.* **1996**, *118*, 8604. l) T. Senga, K. Kamoshida, L. A. Kushch, G. Saito, T. Inayoshi, I. Ono, *Mol. Cryst. Liq. Cryst.* **1997**, *296*, 97. m) G. Saito, S. S. Pac, O. O. Drozdova, *Synth. Met.* **2001**, *120*, 667. n) G. Saito, S. Hirate, K. Nishimura, H. Yamochi, *J. Mater. Chem.* **2001**, *11*, 723. o) S.-S. Pac, G. Saito, *J. Solid State Chem.* **2002**, *168*, 486. p) K. Nishimura, S. S. Khasanov, G. Saito, *J. Mater. Chem.* **2002**, *12*, 1693. q) A. Ota, H. Yamochi, G. Saito, *Mol. Cryst. Liq. Cryst.* **2002**, *376*, 177. r) G. Saito, H. Sasaki, T. Aoki, Y. Yoshida, A. Otsuka, H. Yamochi, O. O. Drozdova, K. Yakushi, H. Kitagawa, T. Mitani, *J. Mater. Chem.* **2002**, *12*, 1640. s) G. Saito, H. Yamochi, M. Maesato, Y. Yoshida, A. Ota, Y. Shimizu, *NATO Sci. Ser., II* **2004**, *139*, 19.

17 a) Z. G. Soos, *Annu. Rev. Phys. Chem.* **1974**, *25*, 121. b) J. B. Torrance, in *Molecular Metals*, ed. by W. E. Hatfield, Plenum Pub. Co., **1979**, pp. 7–14. c) J. B. Torrance, *Acc. Chem. Res.* **1979**, *12*, 79. d) J. Tanaka, C. Tanaka, *Mol. Cryst. Liq. Cryst.* **1985**, *126*, 121. e) D. O. Cowan, J. A. Fortkork, R. M. Metzger, in *Lower-Dimensional Systems and Molecular Electronics*, ed. by R. M. Metzger, P. Day, G. C. Papavassiliou, Plenum Press, New York, **1991**, pp. 1–22. f) P. Delhaes, in *Lower-Dimensional Systems and Molecular Electronics*, ed. by R. M. Metzger, P. Day, G. C. Papavassiliou, Plenum Press, New York, **1991**, pp. 43–65.

18 G. Saito, Y. Yoshida, *Bull. Chem. Soc. Jpn.* **2007**, *80*, 1.

19 G. Saito, T. Murata, *Philos. Trans. R. Soc., A* **2008**, *366*, 139.

20 a) W. S. Rapson, D. H. Saunder, E. T. Stewart, *J. Chem. Soc.* **1946**, 1110. b) K. Abe, Y. Matsunaga, G. Saito, *Bull. Chem.*

Soc. Jpn. **1968**, *41*, 2852.

21 a) D. V. Konarev, I. S. Neretin, Yu. L. Slovokhotov, A. L. Litvinov, A. Otsuka, R. N. Lyubovskaya, G. Saito, *Synth. Met.* **2002**, *131*, 87. b) A. Izuoka, T. Tachikawa, T. Sugawara, Y. Suzuki, M. Konno, Y. Saito, H. Shinohara, *J. Chem. Soc., Chem. Commun.* **1992**, 1472.

22 a) M. Sakata, M. Maesato, G. Saito, T. Yamamoto, K. Yakushi, S. S. Khasanov, N. G. Spitsina, A. D. Dubrovskii, E. G. Yagubskii, P. Deplano, M. L. Mercuri, in *Multifunctional Conducting Molecular Materials*, ed. by G. Saito, F. Wudl, R. C. Haddon, K. Tanigaki, T. Enoki, H. E. Katz, M. Maesato, RSC Publishing, **2007**, pp. 91–96. b) H. M. Yamamoto, J.-I. Yamaura, R. Kato, *J. Am. Chem. Soc.* **1998**, *120*, 5905.

23 a) R. P. Shibaeva, V. P. Kaminskii, E. B. Yagubskii, *Mol. Cryst. Liq. Cryst.* **1985**, *119*, 361. b) T. Mori, H. Inokuchi, Y. Misaki, T. Yamabe, H. Mori, S. Tanaka, *Bull. Chem. Soc. Jpn.* **1994**, *67*, 661. c) M. Ashizawa, A. Akutsu, B. Noda, H. Nii, T. Kawamoto, T. Mori, T. Nakayashiki, Y. Misaki, K. Tanaka, K. Takimiya, T. Otsubo, *Bull. Chem. Soc. Jpn.* **2004**, *77*, 1449. d) K. Takimiya, A. Ohnishi, Y. Aso, T. Otsubo, F. Ogura, K. Kawabata, K. Tanaka, M. Mizutani, *Bull. Chem. Soc. Jpn.* **1994**, *67*, 766.

24 Y. Matsunaga, *Bull. Chem. Soc. Jpn.* **1969**, *42*, 2490.

25 a) J. B. Torrance, J. E. Vazquez, J. J. Mayerle, V. Y. Lee, *Phys. Rev. Lett.* **1981**, *46*, 253. b) An appropriate V-shaped line for the TCNQ system was obtained by a parallel shift of the V-shaped line for the *p*-quinone system towards the lower side by 0.13–0.16 V (Ref. 18).

26 H. M. McConnell, B. M. Hoffman, R. M. Metzger, *Proc. Natl. Acad. Sci. U.S.A.* **1965**, *53*, 46.

27 a) Y. Matsunaga, VII Molecular Crystals Symposium, Nikko, Japan, **1975**. b) J. O. Williams, *Adv. Phys. Org. Chem.* **1978**, *16*, 159.

28 *Semiconductors and Semimetals*, ed. by E. Conwell, Academic Press, New York, **1988**, Vol. 27.

29 J. Fraxedas, *Molecular Organic Materials from Molecules to Crystalline Solids*, Cambridge University Press, Cambridge UK, **2006**.

30 a) D. Jérome, H. J. Schulz, *Adv. Phys.* **1982**, *31*, 299. b) D. Jérome, *Science* **1991**, *252*, 1509.

31 *The Physics of Organic Superconductors and Conductors*, ed. by A. G. Lebed, Springer-Verlag, Berlin, **2008**.

32 a) H. Urayama, T. Inabe, T. Mori, Y. Maruyama, G. Saito, *Bull. Chem. Soc. Jpn.* **1988**, *61*, 1831. b) C. Katayama, M. Honda, H. Kumagai, J. Tanaka, G. Saito, H. Inokuchi, *Bull. Chem. Soc. Jpn.* **1985**, *58*, 2272.

33 a) Md. B. Zaman, J. Toyoda, Y. Morita, S. Nakamura, H. Yamochi, G. Saito, K. Nishimura, N. Yoneyama, T. Enoki, K. Nakasuji, *J. Mater. Chem.* **2001**, *11*, 2211. b) K. Nishimura, G. Saito, G. G. Abashev, A. G. Tenishev, *Synth. Met.* **2001**, *120*, 911.

34 O. Drozdova, H. Yamochi, K. Yakushi, M. Uruichi, S. Horiuchi, G. Saito, *J. Am. Chem. Soc.* **2000**, *122*, 4436.

35 a) T. J. Emge, F. M. Wiygul, J. S. Chappell, A. N. Bloch, J. P. Ferraris, D. O. Cowan, T. J. Kistenmacher, *Mol. Cryst. Liq. Cryst.* **1982**, *87*, 137. b) T. J. Kistenmacher, T. J. Emge, A. N. Bloch, D. O. Cowan, *Acta Crystallogr., Sect. B* **1982**, *38*, 1193.

36 J. R. Andersen, R. A. Craven, J. E. Weidenborner, E. M. Engler, *J. Chem. Soc., Chem. Commun.* **1977**, 526.

37 a) M. Mizuno, A. F. Garito, M. P. Cava, *J. Chem. Soc., Chem. Commun.* **1978**, 18. b) T. Mori, H. Inokuchi, *Solid State Commun.* **1986**, *59*, 355. c) T. Mori, H. Inokuchi, *Bull. Chem. Soc. Jpn.* **1987**, *60*, 402. d) Y. Iwasa, K. Mizuhashi, T. Koda, Y. Tokura, G. Saito, *Phys. Rev. B* **1994**, *49*, 3580. e) H. M. Yamamoto, M. Hagiwara, R. Kato, *Synth. Met.* **2003**, *133–134*, 449.

38 G. Saito, T. Enoki, K. Toriumi, H. Inokuchi, *Solid State Commun.* **1982**, *42*, 557.

39 a) *J. Phys: Conf. Ser.* **2009**, *148*. b) *Photoinduced Phase Transitions*, ed. by K. Nasu, World Scientific Publishing Co. Pte. Ltd., Singapole, **2004**.

40 a) J. B. Torrance, Y. Tomkiewicz, R. Bozio, C. Pecile, C. R. Wolfe, K. Bechgaard, *Phys. Rev. B* **1982**, *26*, 2267. b) T. J. Emge, D. O. Cowan, A. N. Bloch, T. J. Kistenmacher, *Mol. Cryst. Liq. Cryst.* **1983**, *95*, 191.

41 a) J. W. Bray, H. R. Hart, Jr., L. V. Interrante, I. S. Jacobs, J. S. Kasper, G. D. Watkins, S. H. Wee, J. C. Bonner, *Phys. Rev. Lett.* **1975**, *35*, 744. b) J. W. Bray, L. V. Interrante, I. S. Jacobs, J. C. Bonner, in *Extended Linear Chain Compounds*, ed. by J. S. Miller, Plenum, New York, **1983**, Vol. 3, p. 253.

42 a) Y. Tokura, S. Koshihara, Y. Iwasa, H. Okamoto, T. Komatsu, T. Koda, N. Iwasawa, G. Saito, *Phys. Rev. Lett.* **1989**, *63*, 2405. b) F. Kagawa, S. Horiuchi, M. Tokunaga, J. Fujioka, Y. Tokura, *Nat. Phys.* **2010**, *6*, 169.

43 a) J. S. Miller, A. J. Epstein, W. M. Reiff, *Chem. Rev.* **1988**, *88*, 201. b) J. S. Miller, A. J. Epstein, *Coord. Chem. Rev.* **2000**, *206–207*, 651. c) P.-M. Allemand, K. C. Khemani, A. Koch, F. Wudl, K. Holczer, S. Donovan, G. Grüner, J. D. Thompson, *Science* **1991**, *253*, 301.

44 a) H. Imai, T. Inabe, T. Otsuka, T. Okuno, K. Awaga, *Phys. Rev. B* **1996**, *54*, R6838. b) T. Komatsu, N. Kojima, G. Saito, *Solid State Commun.* **1997**, *103*, 519. c) M. Fourmigué, B. Domercq, I. V. Jourdain, P. Molinié, F. Guyon, J. Amaudrut, *Chem.—Eur. J.* **1998**, *4*, 1714. d) E. Ribera, C. Rovira, J. Veciana, J. Tarrés, E. Canadell, R. Rousseau, E. Molins, M. Mas, J.-P. Schoeffel, J.-P. Pouget, J. Morgado, R. T. Henriques, M. Almeida, *Chem.—Eur. J.* **1999**, *5*, 2025. e) S. Nishihara, T. Akutagawa, T. Hasegawa, T. Nakamura, *Chem. Commun.* **2002**, 408.

45 a) T. Mori, H. Mori, S. Tanaka, *Bull. Chem. Soc. Jpn.* **1999**, *72*, 179. b) H. Mori, S. Tanaka, T. Mori, A. Kobayashi, H. Kobayashi, *Bull. Chem. Soc. Jpn.* **1998**, *71*, 797. c) H. Mori, S. Tanaka, T. Mori, *Phys. Rev. B* **1998**, *57*, 12023. d) J. Ouyang, K. Yakushi, Y. Misaki, K. Tanaka, *Phys. Rev. B* **2001**, *63*, 054301. e) K. Yamamoto, K. Yakushi, K. Miyagawa, K. Kanoda, A. Kawamoto, *Phys. Rev. B* **2002**, *65*, 085110.

46 a) spin-Peierls systems of TMTTF salts are included in the phase diagram by D. Jerome (Ref. 31b). b) spin-Peierls systems of BEDT-TTF salts are summarized in Table 12 and on p. 30 in Ref. 18. DBTTF·Cl_2TCNQ showed Peierls transition at 180 K then spin-Peierls one at 38 K. c) C. S. Jacobsen, H. J. Pedersen, K. Mortensen, K. Bechgaard, *J. Phys. C: Solid State Phys.* **1980**, *13*, 3411.

47 U. Welp, S. Fleshler, W. K. Kwok, G. W. Crabtree, K. D. Carlson, H. H. Wang, U. Geiser, J. M. Williams, V. M. Hitsman, *Phys. Rev. Lett.* **1992**, *69*, 840.

48 Y. Shimizu, K. Miyagawa, K. Kanoda, M. Maesato, G. Saito, *Phys. Rev. Lett.* **2003**, *91*, 107001.

49 a) N. Yoneyama, A. Miyazaki, T. Enoki, G. Saito, *Bull. Chem. Soc. Jpn.* **1999**, *72*, 639. b) T. Ise, T. Mori, K. Takahashi, *J. Mater. Chem.* **2001**, *11*, 264.

50 a) H. Okamoto, T. Mitani, Y. Tokura, S. Koshihara, T. Komatsu, Y. Iwasa, T. Koda, G. Saito, *Phys. Rev. B* **1991**, *43*, 8224. b) M. Le Cointe, M. H. Lemée-Cailleau, H. Cailleau, B. Toudic, L. Toupet, G. Heger, F. Moussa, P. Schweiss, K. H. Kraft, N. Karl, *Phys. Rev. B* **1995**, *51*, 3374. c) S. A. Bewick, R. A. Pascal, D. M. Ho, Z. G. Soos, M. Masino, A. Girlando, *J. Chem. Phys.* **2005**, *122*, 024710.

51 For 1,6-diaminopyrene•*p*-haloanils: a) P. L. Kronick, H. Scott, M. M. Labes, *J. Chem. Phys.* **1964**, *40*, 890. b) Y. Matsunaga, *Nature* **1966**, *211*, 183. c) H. Goto, T. Fujinawa, H. Asahi, T. Inabe, H. Ogata, S. Miyajima, Y. Maruyama, *Bull. Chem. Soc. Jpn.*, **1996**, *69*, 85. For 2:1 DDA complex of 2,3-dimethylanthra[1,9-*c*,*d*:4,10-*c*′,*d*′]diselenole•Me_2TCNQ: d) K. Takimiya, Y. Aso, T. Otsubo, F. Ogura, *Bull. Chem. Soc. Jpn.* **1991**, *64*, 2091.

52 Section 4.7.1 and Table 30 in Ref. 18.

53 a) Section 4.2 in Ref. 18. b) S. Horiuchi, R. Kumai, Y. Tokura, *Angew. Chem., Int. Ed.* **2007**, *46*, 3497. c) S. Horiuchi, F. Ishii, R. Kumai, Y. Okimoto, H. Tachibana, N. Nagaosa, Y. Tokura, *Nat. Mater.* **2005**, *4*, 163.

54 a) T. Hasegawa, S. Kagoshima, T. Mochida, S. Sugiura, Y. Iwasa, *Solid State Commun.* **1997**, *103*, 489. b) T. Hasegawa, K. Inukai, S. Kagoshima, T. Sugawara, T. Mochida, S. Sugiura, Y. Iwasa, *Synth. Met.* **1997**, *86*, 1801.

55 T. Sugano, K. Yakushi, H. Kuroda, *Bull. Chem. Soc. Jpn.*, **1978**, *51*, 1041. However, B-band definitely appears in the charge ordered stripe of 0110: O. Drozdova, K. Yakushi, K. Yamamoto, A. Ota, H. Yamochi, G. Saito, H. Tashiro, D. B. Tanner, *Phys. Rev. B* **2004**, *70*, 075107.

56 a) D. Chasseau, J. Gaultier, G. Hauw, *C. R. Acad. Sci., Ser. C* **1972**, *274*, 1434. b) D. Chasseau, J. Gaultier, G. Hauw, M. Schroener, *C. R. Acad. Sci., Ser. C* **1972**, *275*, 1491. c) R. M. Metzger, N. E. Heimer, D. Gundel, H. Sixl, R. H. Harms, H. J. Keller, D. Nöthe, D. Wehe, *J. Chem. Phys.* **1982**, *77*, 6203. d) D. Gundel, H. Sixl, R. M. Metzger, N. E. Heimer, R. H. Harms, H. J. Keller, D. Nöthe, D. Wehe, *J. Chem. Phys.* **1983**, *79*, 3678. e) M. C. Grossel, F. A. Evans, J. A. Hriljac, K. Prout, S. C. Weston, *J. Chem. Soc., Chem. Commun.* **1990**, 1494. f) M. C. Grossel, S. C. Weston, *Chem. Mater.* **1996**, *8*, 977. g) A. Singhabhandhu, P. D. Robinson, J. H. Fang, W. E. Geiger, Jr., *Inorg. Chem.* **1975**, *14*, 318. h) F. Iwasaki, S. Hironaka, N. Yamazaki, K. Kobayashi, *Bull. Chem. Soc. Jpn.*, **1992**, *65*, 2180. The high conductivity of ca. 5 S cm^{-1} at RT cannot be rationalized based on its full ionicity and non-segregated stacking manner. If one looks at Fig. 2 of this paper, a kind of segregated stacking of $\cdots$AAAA$\cdots$ is seen. So, a reexamination of the ionicity of the component molecules in this material would be necessary. i) K. J. Kilgore, N. P. Rath, M. T. Jones, *Mater. Res. Soc. Symp. Proc.* **1992**, *247*, 529. j) A. Dolbecq, M. Fourmigue, P. Batail, C. Coulon, *Chem. Mater.* **1994**, *6*, 1413. k) D. A. Clemente, A. Marzotto, *J. Mater. Chem.* **1996**, *6*, 941. l) P. Erk, S. Hünig, G. Klebe, M. Krebs, J. U. von Schütz, *Chem. Ber.* **1991**, *124*, 2005. m) T. Mori, P. Wu, K. Imaeda, T. Enoki, H. Inokuchi, G. Saito, *Synth. Met.* **1987**, *19*, 545. n) N. Iwasawa, H. Urayama, H. Yamochi, G. Saito, K. Imaeda, T. Mori, Y. Maruyama, H. Inokuchi, T. Enoki, Y. Higuchi, N. Yasuoka, *Synth. Met.* **1988**, *27*, 463. o) K. Imaeda, T. Mori, C. Nakano, H. Inokuchi, N. Iwasawa, G. Saito, *Bull. Chem. Soc. Jpn.* **1991**, *64*, 2159.

57 a) A. B. Harris, R. V. Lange, *Phys. Rev.* **1967**, *157*, 295. b) M. J. Rice, *Solid State Commun.* **1979**, *31*, 93. c) C. S. Jacobsen, in *Semiconductors and Semimetals*, ed. by E. Conwell, Academic Press, New York, **1988**, Chap. 5.

58 R. Bozio, I. Zanon, A. Girlando, C. Pecile, *J. Chem. Phys.* **1979**, *71*, 2282.

59 M. Meneghetti, R. Bozio, I. Zanon, C. Pecile, C. Ricotta, M. Zanetti, *J. Chem. Phys.* **1984**, *80*, 6210.

60 M. Meneghetti, R. Bozio, C. Pecile, *J. Phys. (Paris)* **1986**, *47*, 1377.

61 E. Demiralp, S. Dasgupta, W. A. Goddard, III, *J. Phys. Chem. A* **1997**, *101*, 1975.

62 K. I. Pokhodnia, M. E. Kozlov, V. G. Onischenko, D. Schweitzer, J. Moldenhauer, R. Zamboni, *Synth. Met.* **1993**, *56*, 2364.

63 J. S. Chappell, A. N. Bloch, W. A. Bryden, M. Maxfield, T. O. Poehler, D. O. Cowan, *J. Am. Chem. Soc.* **1981**, *103*, 2442. It should be noted, however, that the authors of this paper used both b_{1u} and a_g modes of C≡N stretching in their analysis. If one uses only b_{1u} modes of IR spectra, the linear relation between $\nu_{C\equiv N}$ and the degree of CT (δ) is held only below $\delta = 0.5$.

64 R. P. Shibaeva, L. P. Rosenberg, *Kristallografiya* **1981**, *26*, 1224.

65 a) A. Otsuka, G. Saito, T. Sugano, M. Kinoshita, K. Honda, *Thin Solid Films* **1989**, *179*, 259. b) A. Otsuka, H. Yamochi, G. Saito, T. Sugano, M. Kinoshita, S. Sato, K. Honda, K. Ohfuchi, M. Konno, *Synth. Met.* **1991**, *42*, 1699. c) J. Yamaura, A. Miyazaki, T. Enoki, G. Saito, *Phys. Rev. B* **1997**, *55*, 3649.

66 a) O. O. Drozdova, V. N. Semkin, R. M. Vlasova, N. D. Kushch, E. B. Yagubskii, *Synth. Met.* **1994**, *64*, 17. b) G. Visentini, M. Masino, C. Bellitto, A. Girlando, *Phys. Rev. B* **1998**, *58*, 9460.

67 N. Ueda, Y. Sakata, S. Misumi, *Bull. Chem. Soc. Jpn.* **1986**, *59*, 3289.

68 T. Yumoto, T. Akutagawa, T. Hasegawa, T. Nakamura, H. Ikegami, G. Saito, *Synth. Met.* **1999**, *102*, 1733.